L- and *D*-proline thiosemicarbazone conjugates: coordination behavior in solution, and the effect of copper(II) coordination on their antiproliferative activity

Miljan N. M. Milunovic,[a] Éva A. Enyedy,[b] Nóra V. Nagy,[c] Tamás Kiss,[b,d] Robert Trondl,[a] Michael A. Jakupec,[a] Bernhard K. Keppler,[a] Regina Krachler,[a] Ghenadie Novitchi,[e] Vladimir B. Arion*[a]*

[a]*University of Vienna, Institute of Inorganic Chemistry, Währinger Strasse 42, A-1090 Vienna, Austria,* [b]*Department of Inorganic and Analytical Chemistry, University of Szeged, Dóm tér 7. H-6720 Szeged, Hungary,* [c]*Institute of Molecular Pharmacology, Research Centre for Natural Sciences, Hungarian Academy of Sciences, Pusztaszeri út 59-67, H-1025, Budapest, Hungary,* [d]*Bioinorganic Chemistry Research Group of the Hungarian Academy of Sciences, University of Szeged, Dóm tér 7. H-6720 Szeged, Hungary,* [e]*Laboratoire National des Champs Magnétiques Intenses, CNRS UPR-3228, 25 rue des Martyrs, 38042 Grenoble cedex 9, France*

Thiosemicarbazones, Copper(II), Solution equilibrium, Stability constants, Antiproliferative activity

RECEIVED DATE (to be automatically inserted after your manuscript is accepted)

*To whom correspondence should be addressed. E-mail: enyedy@chem.u-szeged.hu (E.A.E.); vladimir.arion@univie.ac.at (V.B.A.).

Abstract

Two enantiomerically pure thiosemicarbazone-proline conjugates with enhanced aqueous solubility, namely 2-hydroxy-3-methyl-(*S*)-pyrrolidine-2-carboxylate-5-methylbenzaldehyde thiosemicarbazone [*L*-Pro-STSC or (*S*)-H_2L] and 2-hydroxy-3-methyl-(*R*)-pyrrolidine-2-carboxylate-5-methylbenzaldehyde thiosemicarbazone [*D*-Pro-STSC or (*R*)-H_2L] have been synthesized and characterized by elemental analysis, spectroscopic methods (UV−vis, ^{1}H and ^{13}C NMR) and ESI mass spectrometry. Metal complexation behavior of *L*-Pro-STSC, stoichiometry and thermodynamic stability of iron(II), iron(III), copper(II) and zinc(II) complexes in 30% (w/w) DMSO/H_2O solvent mixture have been studied by pH-potentiometric, UV−vis spectrophotometric, CD, EPR, ^{1}H NMR spectroscopic and spectrofluorimetric measurements. By reaction of $CuCl_2 \cdot 2H_2O$ with (*S*)-H_2L and (*R*)-H_2L, respectively, the complexes [Cu(*S*-H_2L)Cl]Cl and [Cu(*R*-H_2L)Cl]Cl have been prepared and comprehensively characterized. X-ray diffraction study of [Cu(*R*-H_2L)Cl]Cl showed the formation of a square-planar copper(II) complex, which builds up stacks with interplanar separation of 3.3 Å. The antiproliferative activity of two chiral ligands and their corresponding copper(II) complexes has been tested in two human cancer cell lines, namely SW480 (colon carcinoma) and CH1 (ovarian carcinoma). The thiosemicarbazone-proline conjugates *L*-Pro-STSC and *D*-Pro-STSC show only moderate cytotoxic potency with IC_{50} values of 62 and 75 μM, respectively, in CH1 cells and > 100 μM in SW480 cells. However, the corresponding copper(II) complexes are 13 and 5 times more potent in CH1 cells, based on comparison of IC_{50} values, and in SW480 cells the increase in antiproliferative activity is even higher. In both tested cell lines the *L*-Pro-STSC as well as its copper(II) complex show slightly stronger antiproliferative activity than the compounds with a *D*-Pro moiety, yielding IC_{50} values of 4.6 and 5.5 μM, for [Cu(*L*-Pro-STSC)Cl]Cl in CH1 and SW480 cells, respectively.

Introduction

Thiosemicarbazones (TSCs) are strong chelating ligands for transition metals with a broad spectrum of biological activity.[1,2] α(N)-Heterocyclic TSCs are known as potential antitumor drugs.[3,4] Triapine (3-aminopyridine-2-carboxaldehyde thiosemicarbazone) is the most prominent example of this family of compounds and has been extensively studied as a single agent and in combinations with established drugs in phase I and II clinical trials with mixed results.[5–8] Triapine and other related TSCs, as well as their metal complexes, are known as strong inhibitors of ribonucleotide reductase (RNR), an important enzyme promoting the

production of deoxyribonucleotides required for DNA synthesis and cell proliferation,[9–14] while some copper(II) thiosemicarbazonates inhibit topoisomerase IIα, an enzyme responsible for regulation of DNA topology[15–17] or induce oxidative stress.[18] The formation of an iron(II) complex with Triapine, its reaction with molecular oxygen and subsequent formation of reactive oxygen species (ROS) which destroy the tyrosyl radical of RNR are considered the main steps in their mode of action.[19,20] A potential specific binding pocket for Triapine on the surface of the mouse R2 RNR protein has been proposed quite recently.[21] The ability of TSCs to act as chelators of transition metal ions is well documented in the literature by isolation and characterization of the resulting complexes in the solid state,[22] and, by solution equilibrium studies, which provide valuable information about the chemical species present in aqueous solution at physiological pH and their thermodynamic stability.[23] Studies in solution are of utmost importance for understanding the mechanism of action of biologically active compounds and design of even stronger chelators. However, such investigations are very often hampered by the low aqueous solubility of TSCs.

2-Hydroxybenzaldehyde (or salicylaldehyde) TSC (STSC) was also reported to form complexes with transition metals.[24] However, this organic compound shows only a moderate cytotoxic activity in tumor cells,[25,26] in comparison with α(N)-heterocyclic TSCs exhibiting IC_{50} values in the low micromolar or even high nanomolar range,[27,22f] and the reasons for this dramatic drop in activity are still unknown. The antiproliferative activity of STSC can be enhanced to some extent by attachment of polar, electron-donating substituents, e.g. dimethylamino and/or methoxy group(s) to the 2-hydroxybenzaldehyde moiety[26] or by coordination to metal ions.[25]

Copper(II) chloride forms a square-planar complex with 2-hydroxy-3-methoxybenzaldehyde TSC (HL) of 1:1 stoichiometry, namely $[Cu(L)Cl]\cdot H_2O$.[28] The methoxy group and the co-crystallized water molecule are involved in formation of one-dimensional planar chains via intermolecular hydrogen-bonding interactions. By reaction of copper(II) sulfate with salicylaldehyde-β-D-glycoside TSC followed by re-crystallization of the precipitate from DMSO the complex $[Cu(L^1)(H_2O)]_2SO_4\cdot 2DMSO$, where HL^1 = 2-hydroxybenzaldehyde TSC, was isolated and characterized. The crystal structure consists of centrosymmetric dinuclear cations stabilized by π−π* interaction between four-coordinate square-planar monocations. The X-ray diffraction structures of both copper(II) complexes imply that both species are potential DNA intercalators. Moreover, it has been reported recently, that square-planar

coordination geometry of some copper(II) TSCs is likely the biologically active configuration in Topo-IIα inhibition via an ATP binding site-based mechanism.[16,17]

Reports on thermodynamic stability of the metal complexes of STSC and its derivatives are scarce in the literature,[29] because of their generally low aqueous solubility hampering solution equilibrium studies. Quite recently some of us studied in detail the stoichiometry and thermodynamic stability of iron(II), iron(III), copper(II), zinc(II) and gallium(III) complexes with STSC in water/dimethyl sulfoxide (DMSO) mixture by pH-potentiometric, UV−vis spectrophotometric, EPR, ^{1}H NMR spectroscopic and spectrofluorimetric measurements and compared these data with those for α(N)-heterocyclic TSCs.[23b,c,29] Herein we report on the synthesis and spectroscopic characterization of two enantiomerically pure Pro-STSC conjugates with enhanced aqueous solubility, namely, 2-hydroxy-3-methyl-(S)-pyrrolidine-2-carboxylate-5-methylbenzaldehyde thiosemicarbazone [*L*-Pro-STSC or (*S*)-H_2L] and 2-hydroxy-3-methyl-(R)-pyrrolidine-2-carboxylate-5-methylbenzaldehyde thiosemicarbazone [*D*-Pro-STSC or (*R*)-H_2L] (Scheme 1). Metal complexation behavior of *L*-Pro-STSC, stoichiometry and thermodynamic stability of iron(II) and iron(III), copper(II) and zinc(II) complexes in 30% (w/w) DMSO/H_2O solvent mixture have been studied by pH-potentiometric, UV−vis spectrophotometric, EPR, ^{1}H NMR, CD spectroscopic and spectrofluorimetric measurements. In addition, the isolation and characterization of square-planar copper(II) complexes with enantiomerically pure Pro-STSC conjugates in the solid state are reported. The effect of copper(II) coordination, as well as chirality of the Pro moiety on the antiproliferative activity of conjugates in two human cancer cell lines has been studied as well.

Results and Discussion

Synthesis and characterization of chiral thiosemicarbazones. The chiral thiosemicarbazone-proline conjugates have been prepared in three steps as shown in Scheme 1. First 3-chloromethyl-2-hydroxy-5-methylbenzaldehyde[30] was allowed to react with *L*- or *D*-proline methyl ester hydrochloride in the presence of triethylamine with formation of compounds (*S*)-**1** and (*R*)-**1**, respectively. Condensation reactions of these latter compounds with thiosemicarbazide followed by hydrolysis of the methyl ester groups afforded the corresponding TSCs with coupled via a methylene group Pro moiety [(*S*)-H_2L and (*R*)-H_2L]. The formation of desired species has been confirmed by ^{1}H and ^{13}C NMR measurements, as well as by ESI mass spectra. The number of ^{1}H and ^{13}C resonances in NMR spectra is in

accord with the proposed structure of C_1 point symmetry. The mass spectra recorded in positive ion mode showed peaks at *m*/*z* 359 and 337 due to $[M+Na]^+$ and $[M+H]^+$ ions, respectively. The pH-metric titrations (vide infra) suggest that *L*-Pro-STSC is tribasic in the studied pH-range and adopts a zwitterionic structure as shown in Scheme 2.

Scheme 1. Synthesis of chiral thiosemicarbazone-proline derivatives (*S*)-**H_2L** and (*R*)-**H_2L**.[a]

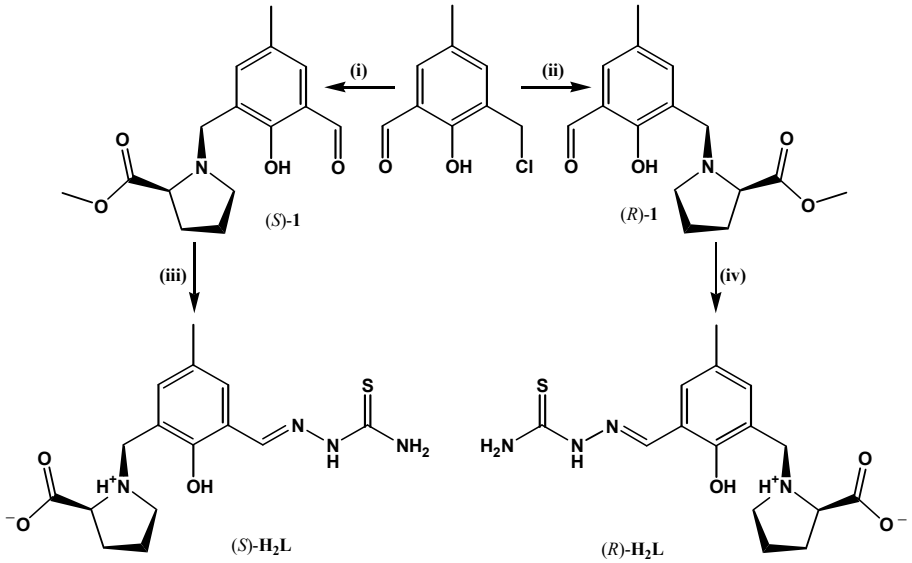

[a]Reagents and conditions: (i) methyl (*S*)-pyrrolidine-2-carboxylate hydrochloride, triethylamine, THF/CH_2Cl_2 1.5:1, rt, purification by column chromatography [(*S*)-**1**, 51%]; (ii) methyl (*R*)-pyrrolidine-2-carboxylate hydrochloride, triethylamine, THF/CH_2Cl_2 1.5:1, rt, purification by column chromatography [(*R*)-**1**, 39%]; (iii) thiosemicarbazide, EtOH/H_2O 1:1, 70–75 °C, 75 h, [(*S*)-**H_2L**, 41%]; (iv) thiosemicarbazide, EtOH/H_2O 1:1, 70–75 °C, 12 h, [(*R*)-**H_2L**, 18%].

Scheme 2. Deprotonation steps of H_3L^+ (relevant for both Pro-STSC enantiomers).[a]

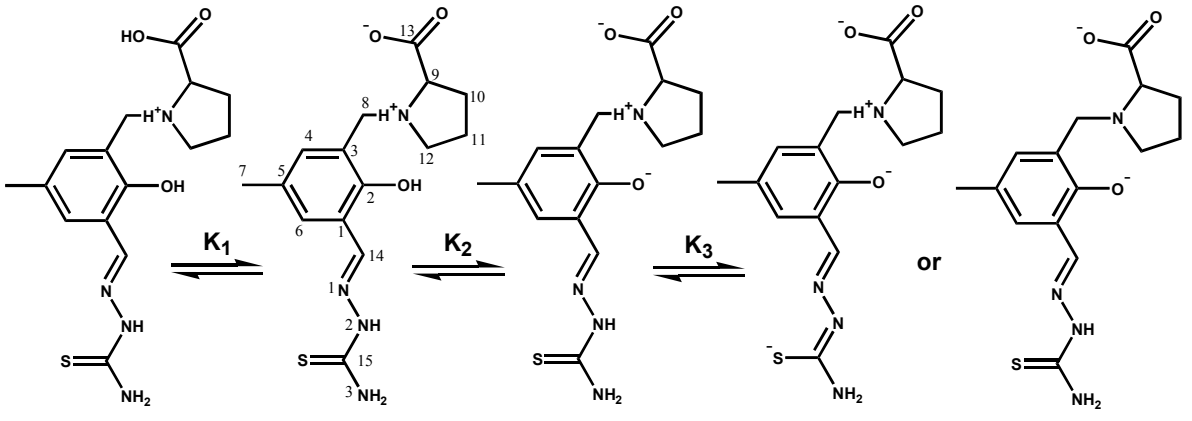

[a] Atom labeling was introduced for assignment of proton resonances.

Aqueous solutions of *L*- and *D*-Pro-STSC ligands at neutral pH are indeed optically active and show Cotton effects for both enantiomers (see Figure S1A). As expected they are roughly mirror images over the 240−400 nm region of the circular dichroism (CD) spectra, while their UV–vis spectra are identical.

Synthesis and characterization of [Cu(*S*-H_2L)Cl]Cl and [Cu(*R*-H_2L)Cl]Cl. By reaction of methanolic solution of $CuCl_2 \cdot 2H_2O$ with (*S*)-H_2L and (*R*)-H_2L the complexes [Cu(*S*-H_2L)Cl]Cl and [Cu(*R*-H_2L)Cl]Cl have been isolated in 55 and 84% yield, respectively. The positive ion ESI mass spectra showed the presence of a strong peak at *m*/*z* 398 attributed to $[Cu(II)(HL)]^+$. In the negative ion mass spectra ions with *m*/*z* 396 and 432 due to $[Cu(II)(L-H)]^-$ and $[Cu(II)LCl]^-$, respectively, were observed. The protonation form of the Pro-STSC ligand adopted in the prepared copper(II) complexes has been unequivocally established by X-ray diffraction study of [Cu(II)(*R*-H_2L)Cl]Cl. Note that for the charge neutral coordinated ligand in this complex we use for consistency the same abbreviation H_2L, although the charge distribution differs from that shown in Scheme 2.

The CD spectra of both copper(II) complexes of *L*-Pro-STSC and *D*-Pro-STSC were recorded at pH 7.4 in the UV range in pure aqueous solution (Figure S1B), which clearly show the presence of enantiomerically pure species.

X-ray Crystallography. X-ray diffraction quality crystals were obtained by slow diffusion of diethyl ether into methanolic solution of [Cu(*R*-H_2L)Cl]Cl**.** The result of X-ray diffraction study of [Cu(*R*-H_2L)Cl]Cl is shown in Figure 1. The complex crystallizes in the non-centrosymmetric monoclinic space group $P2_1$ with two crystallographically independent ionic complexes in the asymmetric unit. The copper(II) ion has a square-planar coordination geometry. The multidentate ligand (H_2L) uses only in part its donor capacity and acts in the complex as a tridentate one, binding to Cu^{2+} via phenolate oxygen O1a, imine nitrogen N1a and thione atom S1a. The bond length C8a−S1a of 1.698(6) is equal within 3 σ with that in $[Cu(L)Cl] \cdot H_2O$,[28] where HL = 2-hydroxy-3-methoxybenzaldehyde thiosemicarbazone. The fourth position in the coordination polyhedron is occupied by a chlorido ligand. In addition, the thiosemicarbazone ligand is protonated at proline nitrogen atom N4a. Protonation is corroborated by difference Fourier map and by the presence of intramolecular bifurcated

hydrogen bonding interaction N4a−H···O1a [N4a···O1a 2.695(5) Å, N4a−H···O1a 131.1°] and N4a−H···O2a [N4a···O2a 2.696(5) Å, N4a−H···O2a 113.8°]. The nitrogen atom N2a acts as proton donor in hydrogen bonding interaction N2a−H···Cl2 [N2a···Cl2 3.072(5) Å, N2a−H···Cl2 147.9°], while O3a in H-bond O3a−H···Cl1a^{i} [O3a···Cl1a^{i} 3.038(4) Å, O3a−H···Cl1a^{i} 171.1°], where *i* denotes symmetry related Cl1a atom generated via symmetry code $x-1$, y, z. Other hydrogen bonding interactions are shown in the unit cell plot in Figure S2. The two crystallographically independent complex cations form stacks in the crystal via π-π* interactions with interplanar separation of about 3.3 Å as shown in Figure S3. All this implies that copper(II) complexes can be considered as potential DNA intercalators similarly to other square-planar metal complexes with chemically related ligands.[31]

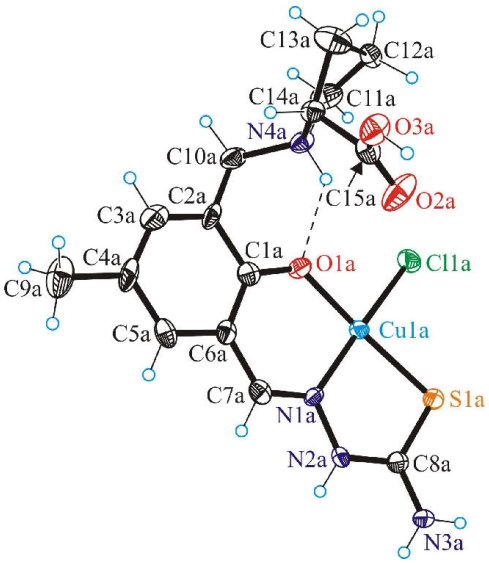

Figure 1. ORTEP view of one of the crystalloghraphically independent cations [Cu(*R*-H_2L)Cl]$^{+}$ with thermal displacement ellipsoids drawn at 50% probability level. Selected bond distances (Å) and bond angles (deg): Cu1a−Cl1a 2.2669(16), Cu1a−S1a 2.2256(15), Cu1a−O1a 1.887(3), Cu1a−N1a 1.956(4), C1a−O1a 1.321(7), C1a−C6a 1.404(8), C6a−C7a 1.422(7), C7a−N1a 1.291(7), N1a−N2a 1.392(6), N2a−C8a 1.336(7), C8a−S1a 1.706(6), C8a−N3a 1.311(6), C15a−O2a 1.193(6), C15a−O3a 1.330(5); O1a−Cu1a−N1a 92.17(17), N1a−Cu1a−S1a 87.26(13), S1a−Cu1a−Cl1a 90.44(6), O1a−Cu1a−Cl1a 90.49(12).

Solution Chemistry

Proton dissociation processes and lipophilicity. Proton-dissociation processes of (*S*)-H_2L (Scheme 2) were followed by pH-potentiometry, UV–vis spectrophotometry and spectrofluorimetry as well as ^{1}H NMR titrations. Measurements were performed in a 30%

(w/w) DMSO/H_2O solvent mixture. Consecutive titrations showed that no ligand decomposition occurred in the pH range studied under the argon atmosphere. Three proton dissociation constants could be determined by different methods (Table 1) and constants obtained are in reasonably good agreement. pK_1 can presumably be attributed to deprotonation of the carboxylic group in (*S*)-H_3L^+, while pK_2 belongs presumably to the phenolic OH. pK_3 can be related to the proton dissociation of the N^2–H group of the thiosemicarbazide moiety or proton dissociation of the tertiary Pro nitrogen. Based on the methods used we cannot distinguish these most probably overlapping deprotonation processes. It is worth noting that the magnitudes of pK_1 and pK_3 values, low and high, respectively, hamper their accurate determination by pH-metry as these deprotonation steps take place in the pH ranges where the pH measurements become uncertain.

Table 1. Proton dissociation constants (pK_a) of the ligand *L*-Pro-STSC determined by various methods;[a] λ_{max} and molar absorptivity ($M^{-1}cm^{-1}$) values for ligand species H_2L, HL^-, L^{2-} determined by UV−vis spectrophotometric titrations and calculated chemical shifts (ppm) for H_3L^+, H_2L and HL^- obtained by ^{1}H NMR titrations {T = 298 K, I = 0.10 M (KCl) in 30% (w/w) DMSO/H_2O}.

	pH-metry		UV−vis		^{1}H NMR[b]		
pK_1	2.17(8)		−		2.36(5)		
pK_2	7.90(3)		7.79(8)		7.85(2)		
pK_3	11.88(12)		11.66(10)		−		
	λ_{max} (ε□/$M^{-1}cm^{-1}$)						
H_2L	308 nm (19250); 336 nm (15820)						
HL^-	302 nm (16490); 388 nm (11640)						
L^{2-}	308 nm (14700); 362 nm (12200)						
δ/ppm[b]	$C^{14}H$ (s)	C^4H (s)	C^6H (s)	C^7H_3 (s)	C^8H_2 (d)	C^8H_2 (d)	C^9H (m)
H_3L^+	8.243	7.400	7.320	2.294	3.644	4.195	3.311
H_2L	8.239	7.392	7.319	2.292	3.601	3.975	3.231
HL^-	8.420	7.609	7.043	2.184	3.294	3.743	2.916

[a] The numbers in parentheses are standard uncertainties of the quoted pK_a values. [b] Determined in 30% (w/w) d_6-DMSO/H_2O

The pH-dependent physico-chemical properties of the *L*-Pro-STSC ligand such as fluorescence emission, absorbance, chemical shifts were monitored by different spectroscopic methods with a different level of sensitivity to the certain proton dissociation processes. The UV–vis spectra are almost unchanged in the pH range where the deprotonation of the carboxylic group occurs (Figure 2), thus pK_1 could not be determined by this method with acceptable accuracy. Deprotonation of the phenolic OH is accompanied by a considerable shift of the λ_{max} value from 336 to 388 nm and the colorless solution of the ligand turns into yellow. Two well-separated isosbestic points are seen at 355 and 373 nm due to the deprotonation equilibria $H_2L \rightleftharpoons HL^- + H^+$ and $HL^- \rightleftharpoons L^{2-} + H^+$, respectively. Therefore, pK_2, pK_3 values and the spectra of the individual ligand species (H_2L; HL^-; L^{2-}) (Table 1, Figure S4) were calculated on the basis of deconvolution of the UV–vis spectra.

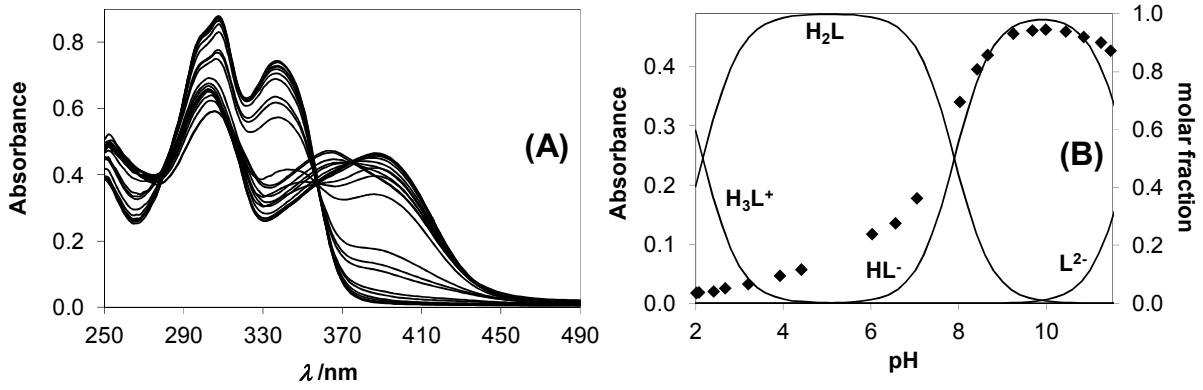

Figure 2. UV−vis spectra of *L*-Pro-STSC at different pH values (A); Concentration distribution curves for ligand species with the pH-dependence of absorbance values at 384 nm (◆) (B) {$c_{ligand} = 4.0 \times 10^{-5}$ M; $T = 298$ K, $I = 0.10$ M (KCl) in 30% (w/w) DMSO/H_2O}.

L-Pro-STSC possesses intrinsic fluorescence due to its extended conjugated electronic system (see Figure 3 and inset for 3D fluorescence spectrum), which is a valuable property for e.g. monitoring cellular uptake or intracellular distribution of the ligand or its metal complexes by fluorescence microscopy. The fluorescence emission of *L*-Pro-STSC in its zwitterionic H_3L^+ or H_2L forms is negligible at any excitation wavelength, however, the proton dissociation at the phenolic OH results in a significant increase of the intensity, which is diminished by the third deprotonation step above pH 10.5 (Figure 3).

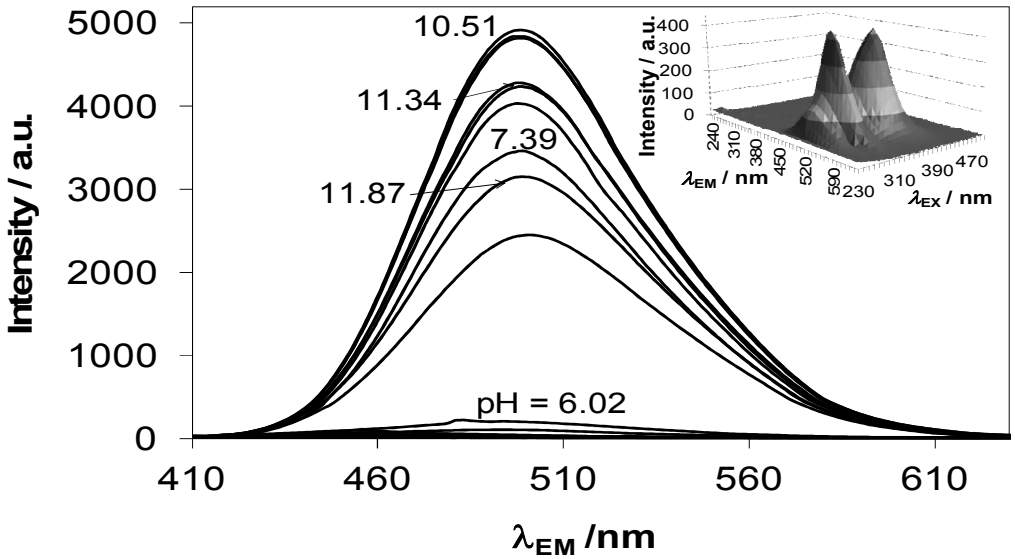

Figure 3. Fluorescence emission spectra of *L*-Pro-STSC at different pH values {$c_{\text{ligand}} = 5.1 \times 10^{-6}$ M; $\lambda_{EX} = 393$ nm; $T = 298$ K, $I = 0.10$ M (KCl) in 30% (w/w) DMSO/H_2O; slits: 5 nm/5 nm}. *Inset shows the 3D fluorescence spectrum at pH 10.0 {slits: 2.5 nm/2.5 nm}.*

The pH-dependent ^{1}H NMR spectra of the ligand (Figure S5) revealed that the protons C^9H and C^8H_2 are most sensitive to the deprotonation of the COOH group. Therefore pK_1 was calculated based on the changes of the chemical shifts (δ) of these protons (Figure 4). The second proton dissociation step is accompanied by significant electronic shielding effects, namely upfield shifts of the C^6H, C^8H_2 and C^9H protons, while the $C^{14}H$ and C^4H resonances were downfield shifted upon increasing the pH (see Figure S5). Further changes were observed at pH > 11 due to the third deprotonation step, but data were not appropriate for calculation of the pK_3 value. We should note here that C^8H_2 protons are displayed in ^{1}H NMR spectra as two doublets because of the non-equivalent orientation in space of the two protons.

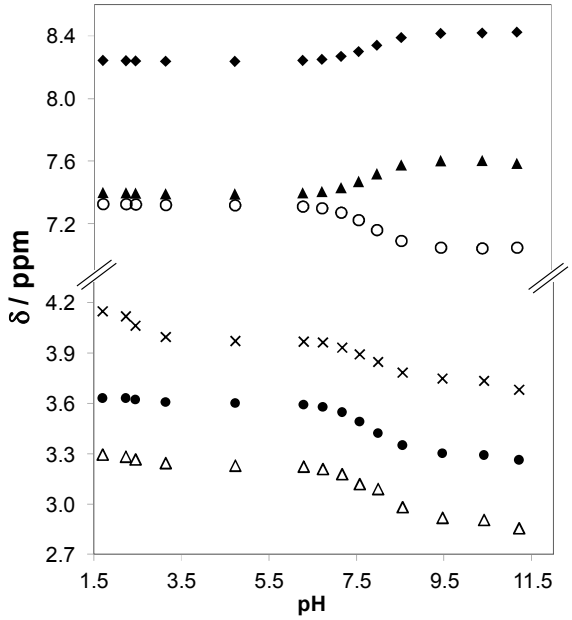

Figure 4. pH-dependence of the chemical shifts (δ) of the various protons of the ligand *L*-Pro-STSC: $C^{14}H$ (♦); $C^{4}H$ (▲); $C^{6}H$ (○); $C^{8}H_2$ (●,×); $C^{9}H$ (Δ) { T = 298 K; I = 0.10 M (KCl) in 30% (w/w) d_6-DMSO/H_2O}. For assignment of particular proton resonances see Scheme 2 and Figure S5.

It should be noted that the phenolic OH of the ligand *L*-Pro-STSC is considerably more acidic compared to that of reference STSC (pK = 8.89[29]). This is presumably due to the formation of a hydrogen bond between the phenolate group and the protonated nitrogen atom of the Pro moiety, which can stabilize the conjugate base, hence decrease the pK.

Distribution coefficients (D) of *L*- and *D*-Pro-STSC were determined at pH 7.4 via the partitioning between *n*-octanol and water (Figure S6). The Pro-STSC conjugates show more hydrophilic character (log$D_{7.4}$ = −0.56 ± 0.01 for the *L*- and −0.60 ± 0.01 for the *D*-enantiomer) compared to the reference STSC (log$D_{7.4}$ = +1.74)[29] or Triapine (log$D_{7.4}$= +0.85).[29] At physiological pH the Pro-STSC ligand is mainly present in the neutral form (75% H_2L, 25% HL^-) and the carboxylic group is fully deprotonated. This relatively low log$D$ value is manifested in enhanced aqueous solubility compared to other chemically related TSCs. The lipophilicity of both complexes was determined via *n*-octanol/water partitioning (Figure S7) at physiological pH. As expected similar log$D_{7.4}$ = +0.25 ± 0.01 and +0.24 ± 0.01 values were obtained for the copper(II) complexes with *L*- and *D*-enantiomer, respectively, showing a more lipophilic character compared to the metal-free ligands. (It should be noted that the distribution coefficients were calculated strictly based on the aqueous

phase spectra and the log$D_{7.4}$ values are equal to their partition coefficients (P) as the neutral [CuL] species predominate at this pH.)

Complexation reactions of copper(II), zinc(II), iron(II) and iron(III) with *L*-Pro-STSC. The complex formation processes of the ligand *L*-Pro-STSC with Cu^{2+}, Zn^{2+}, Fe^{2+} and Fe^{3+} were studied primarily by pH-potentiometry in a 30% (w/w) DMSO/H_2O solvent mixture. The complex formation with Fe^{3+} and Cu^{2+} starts at low pH (pH ~ 2) in the millimolar concentration range, while with Zn^{2+} and Fe^{2+} only at pH > 4, (see Figure 5 for Fe^{2+}). Formation of some mixed hydroxido species occurred at basic pH mainly at 1:1.2 metal-to-ligand ratio, as concluded from the base consumption exceeding the number of dissociable protons in the ligand. The stoichiometries of the metal complexes and the cumulative stability constants furnishing the best fits to the experimental data are listed in Table 2. Stability constant of the species $[Fe(III)LH]^{2+}$ was determined by spectrophotometry on individual samples following the changes of the metal-to-ligand charge transfer (CT) and ligand bands in the region of 300 − 470 nm between pH 1 and 2. Then the determined value was kept constant during the pH-metric data evaluation.

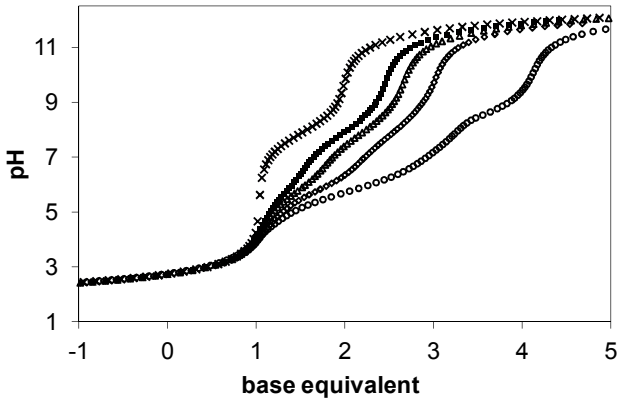

Figure 5. Representative pH-potentiometric titration curves for ligand (×) and for the Fe^{2+} − *L*-Pro-STSC system at 1:1.2 (○), 1:2.3 (◊), 1:3.3 (Δ), 1:4.5 (■) metal-to-ligand ratios {c_{ligand} = 2×10^{-3} M; 30% (w/w) DMSO/H_2O); T = 298 K; I = 0.10 M (KCl)}.

The data reveal formation of merely mono-ligand complexes of Cu^{2+} and Zn^{2+}, while Fe^{2+} and Fe^{3+} ions, in addition, form bis-ligand complexes. Direct comparison of the overall stability constants undoubtedly shows the significantly higher stability of the Fe^{3+} and Cu^{2+} complexes over that of the Zn^{2+} and Fe^{2+} species. pM values have been computed to provide a basis for comparison of the relative chelating ability of *L*-Pro-STSC at physiological pH (Table 2).

(pM stands for the negative logarithm of the equilibrium concentrations of the free metal ion under certain conditions. pM* was also calculated for Fe^{3+} which involves the various hydroxido species $[Fe(III)_pH_r]$, since they belong to the unbound fraction, in addition to the free Fe^{3+} ion).

Table 2. Stability constants ($\log\beta[M_pL_qH_r]$) for the Cu^{2+}, Zn^{2+}, Fe^{2+} and Fe^{3+} complexes of the *L*-Pro-STSC with some stepwise constants and pM values {T = 298 K, I = 0.10 M (KCl) in 30% (w/w) $DMSO/H_2O$}[a].

	Cu^{2+}	Zn^{2+}	Fe^{2+}	Fe^{3+}
$\log\beta([MLH])$	21.58(3)	18.12(3)	18.14(4)	22.39(4)[b]
$\log\beta([ML])$	17.54(3)	12.40(3)	12.24(6)	19.48(3)
$\log\beta([ML_{-1}])$	6.97(4)	2.51(3)	–	–
$\log\beta([ML_2H])$	–	–	28.86(5)	38.24(3)
$\log\beta([ML_2])$	–	–	21.07(6)	33.32(4)
$\log\beta([ML_2H_{-1}])$	–	–	10.99(7)	22.13(8)
fitting parameter (mL)	5.15×10^{-3}	5.52×10^{-3}	8.64×10^{-3}	3.01×10^{-3}
$\log K([ML_2])$[e]	–	–	8.83	13.84
pM[c]	13.4	8.3	8.2	18.9[d]

[a] The numbers in parentheses are standard uncertainties for the stability constants of the complexes. Charges of the complexes are omitted for simplicity (H_2L is charge-neutral). [b] Determined by UV−vis spectrophotometric measurements at pH = 1 − 2. [c] pM (= –log[M]) values at pH = 7.4; $c_M = 1\times10^{-6}$ M; M : L = 1:10. [d] pM* = $-\log(\Sigma[M_pH_r])$ = 10.9 at pH = 7.4; $c_M = 1\times10^{-6}$ M; M : L = 1:10.[e] $K[ML_2]$ stepwise constant is related to the equilibrium: $ML + L \rightleftharpoons ML_2$. The definition of the other overall stability constants is given in the Supporting Information.

According to these pM (pM*) values the ligand effectiveness is varied in the following order at pH 7.4: $Fe^{2+} \sim Zn^{2+} < Fe^{3+} < Cu^{2+}$. It is worth noting that *L*-Pro-STSC shows the formation of similar type of complexes and quite similar pM values with those of its reference model ligand, STSC. However, a slightly higher efficacy of *L*-Pro-STSC is seen in the case of Fe^{3+} and Zn^{2+}.[29] These findings suggest that both ligands coordinate in a similar fashion to the metal centers and the *L*-Pro moiety does not alter significantly the composition and stability of the metal complexes, but improves their aqueous solubility. In order to elucidate the most probable coordination modes of the *L*-Pro-STSC in metal complexes and to confirm the speciation obtained by the pH-potentiometry UV−vis, EPR, CD and ^1H NMR spectroscopies were applied.

Weak bands in the visible wavelength range belong mainly to the d-d transitions of the Cu^{2+}–*L*-Pro-STSC complexes ($\varepsilon_{580nm} \sim 100 - 180\ M^{-1}cm^{-1}$), which are partly overlapped with the S–Cu^{2+} ligand-to-metal CT bands and represent characteristic pH-dependent changes (Figure 6A). The λ_{max} of this band is decreased significantly parallel to the formation of species [CuL] from $[CuLH]^+$. The formation of $[CuLH_{-1}]^-$ is accompanied by a smaller decrease of the λ_{max} along with an increment in the ligand field and change of the coordination mode of the ligand in complexes (Figure 6B). As the ligand is optically active due to the presence of chirality at the proline moiety, CD spectra in the wavelength range 460–650 nm were recorded (Figure 6C). The location of the maxima and minima of peaks shows pH-dependence and parallel changes with the transformation processes of the complexes are seen; e.g. the negative peak is shifted from 650 via 615 to 562 nm as species [CuL] and $[CuLH_{-1}]^-$ are formed.

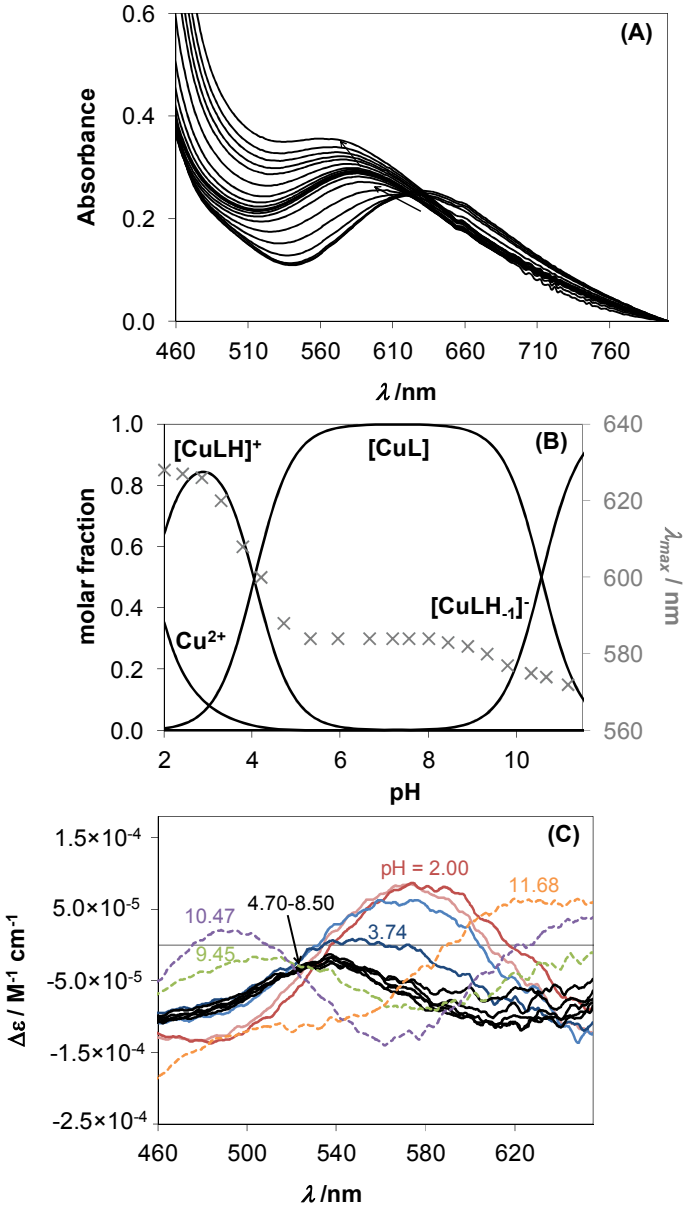

Figure 6. UV–vis spectra of the Cu^{2+} – *L*-Pro-STSC system recorded at different pH values (A) with the corresponding concentration distribution curves calculated with the stability constants obtained by pH-metry depicted together with the λ_{max} values plotted against pH (B) and the pH-dependent CD spectra of the system (C) {$c_M = 2.0 \times 10^{-3}$ M; M:L = 1:1; T = 298 K, I = 0.10 M (KCl) in 30% (w/w) DMSO/H_2O}.

EPR spectra of Cu^{2+}–*L*-Pro-STSC species in 30% (w/w) DMSO/H_2O recorded at various pH values at room temperature (Figure 7) and at 77 K (Figure S8) confirm the speciation obtained by the pH-potentiometry and reveal the coordination modes of the ligand in each Cu^{2+} complex. A two-dimensional simulation of the solution EPR spectra resulted in the individual isotropic EPR parameters of the different Cu^{2+}– *L*-Pro-STSC species (Table 3). The fitted experimental and individual spectra are depicted in Figure 7. The isotropic values calculated by averaging the anisotropic values ($g_{o,calc}$ and $A_{o,calc}$, Table 3) are in good agreement with the corresponding values measured in solution, indicating that the coordination modes adopted by the ligand in solution are preserved upon freezing. The nitrogen hyperfine splitting, caused by the equatorial coordination of one nitrogen atom, is well resolved in all component spectra. The deconvolution of the EPR spectra clearly shows that the species $[CuLH]^+$ predominates in solutions already at pH ~ 2.5 – 3 and with increasing pH the species [CuL] is formed in a wide pH range (pH = 6 − 9), then above pH 10 the species $[CuLH_{-1}]^-$ predominates. No dinuclear or bis-ligand complexes were found under these conditions. Based on the low g_o and high A_o isotropic values the tridentate coordination of *L*-Pro-STSC and nearly square-planar coordination geometry is suggested for all the complexes. In $[CuLH]^+$ coordination of the ligand via phenolate O^-, N^1 and the thione-S, while the hydrazinic N^2–H moiety is still protonated, is the most likely. (The carboxylic group is supposed to be deprotonated in all species in the partly aqueous solution.) Deprotonation of the hydrazinic N^2–H group of the complex results in lower g_o and higher A_o parameters, thus the (O^-, N^1, S^-) binding mode is feasible in the species [CuL]. Further decrease in g_o and increase in A_o values support the deprotonation of the water molecule coordinating in the fourth position of the square-planar complex $[CuLH_{-1}]^-$. Thus this species is regarded as a mixed hydroxido complex, $[CuL(OH)]^-$. Based on EPR data the same coordination modes are realized in the corresponding complexes of *L*-Pro-STSC and STSC,[29] and the carboxylate group of *L*-Pro-STSC is not involved in metal coordination. However, the line width in the component spectra of *L*-Pro-STSC and STSC[29] differs significantly (Figure

7). The broader lines observed for the copper(II) complexes of *L*-Pro-STSC are due to the non-coordinating carboxylate group of the ligand, which leads to a slightly hindered rotation of these complexes in solution. As a consequence, the orientation dependent EPR parameters are not completely averaged out, and the fourth copper line detected in the lower field becomes very broad. Therefore, the simulated spectra, using the equation $\sigma_{MI} = \alpha+\beta M_I+\gamma M_I 2$ for the line width description, showed a systematic deviation from the measured spectra at around 3350 G (Figure 7).

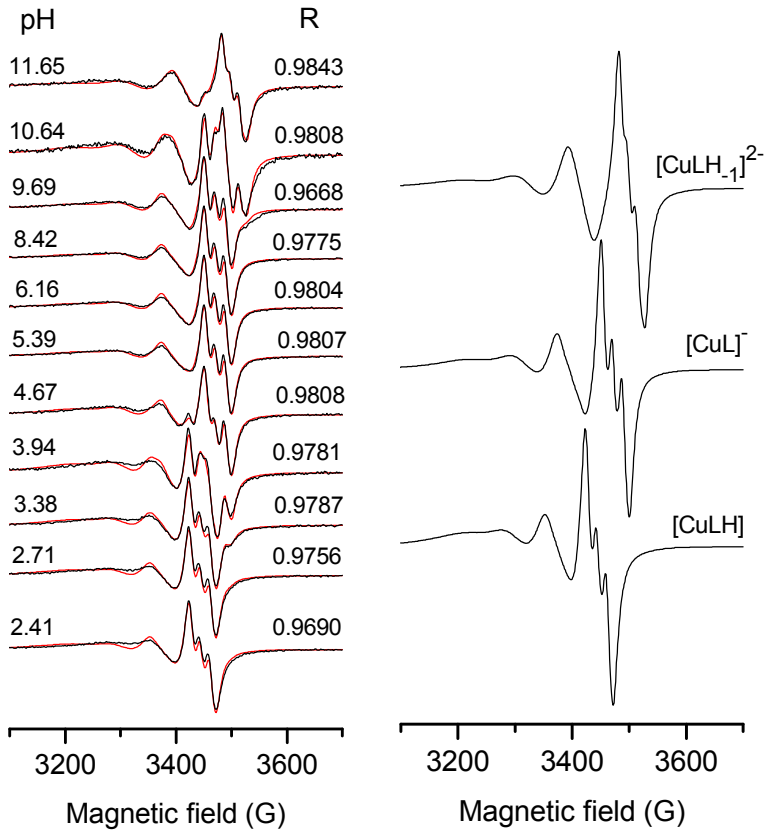

Figure 7. Experimental (black) and simulated (red) EPR spectra for Cu^{2+} – *L*-Pro-STSC system (left) and calculated component spectra for complexes [CuLH], $[CuL]^-$ and $[CuLH_{-1}]^{2-}$ (right) {c_{ligand} = 2 mM; M : L = 1:1; T = 298 K, I = 0.10 M (KCl) in 30% (w/w) $DMSO/H_2O$}.

Table 3. Isotropic EPR parameters of the components obtained for Cu^{2+} – *L*-Pro-STSC system from the two-dimensional simulation of EPR spectra[a,b]

	g_o	A_o /G	a_0^N /G	α / G	β /G	γ /G
Cu^{2+} [c]	2.1970	34.3	–	51.9	−2.2	0.7
$[CuLH]^+$	2.1061(1)	66.1(1)	17.3(1)	35.5(1)	−21.8(1)	3.9(1)

[CuL]	2.0946(1)	76.7(1)	17.5(1)	32.9(1)	−23.0(1)	5.3(1)
$[CuLH_{-1}]^-$	2.0872(2)	84.1(2)	14.9(2)	36.2(1)	−26.5(1)	6.5(1)

[a] The numbers in parentheses are standard uncertainties. [b] Anisotropic EPR parameters for [CuLH]: g_x = 2.0509(1); g_y = 2.0326(1); g_z = 2.2236(1); A_x = 25.4(2) G; A_y = 23.7(2) G; A_z = 170.0(1) G; a_{Nx} = 6.1 G; a_{Ny} = 17.1 G; a_{Nz} = 6.0 G; $g_{0,calc}$ = 2.1024; $A_{0,calc}$ = 75.85 G; for $[CuL]^-$: g_x = 2.0497(1); g_y = 2.0251(1); g_z = 2.2038(1); A_x = 16.3(2) G; A_y = 25.7(2) G; A_z = 176.5(1) G; a_{Nx} = 15.3 G; a_{Ny} = 19.5 G; a_{Nz} = 6.0 G; $g_{0,calc}$ = 2.0929; $A_{0,calc}$ = 75.56 G. [c] Fixed values obtained from separate measurements of Cu^{2+} without ligand.

The tridentate (O^-, N^1, S) coordination mode of Pro-STSC was confirmed by X-ray diffraction structure of [Cu((*R*)-H_2L)Cl]Cl (Figure 1). It should be also noted (based on the stability constants) that the species [CuL] is highly stable even at micromolar concentrations, and practically does not dissociate at physiological pH.

In the Zn^{2+} – *L*-Pro-STSC system analogous complexes with 1:1 metal-to-ligand ratio were detected, although, with considerably lower stability compared to copper(II) species. The speciation model obtained for the zinc(II) complexes was supported by ^{1}H NMR titrations (Figure 8). In the first instance a slow ligand-exchange process was found with respect to the NMR time scale as the chemical shifts of the protons of the metal-free and the bound ligand can be seen separately. At pH < 4 only the peaks of the metal-free ligand are present. A new set of signals can be found additionally with increasing pH, which most probably belongs to the minor protonated complex $[ZnLH]^+$. These signals with a slightly shifted position become predominant between pH 6.5 and 9 where the species [ZnL] is formed. There was no free ligand detected at 1:1 metal-to-ligand ratio at pH > 6.5. Another species, the mixed hydroxido $[ZnLH_{-1}]^-$ (=$[ZnL(OH)]^-$) starts to be formed at pH > 8.5, its proton resonances are well-separated from those of [ZnL] due to relatively slow ligand-exchange equilibrium between them (Figure S9). Distribution of the ligand between the bound and unbound fraction at 1:1 metal-to-ligand ratio was calculated on the basis of the integrated area of the signals of the various ligand protons, and the result is in a good agreement with the concentration distribution curves calculated with the stability constants (Figure 9).

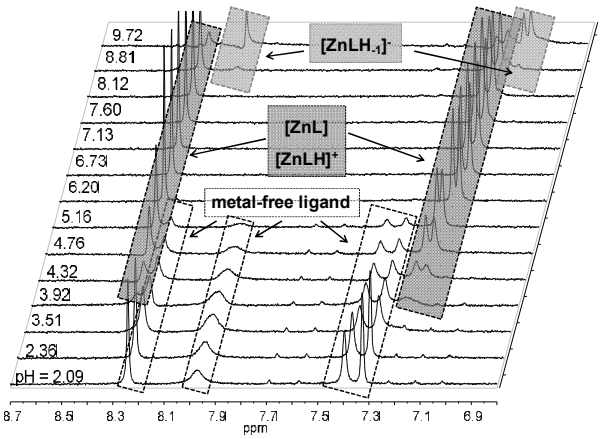

Figure 8. pH-dependent ^{1}H NMR spectra of the Zn^{2+} − *L*-Pro-STSC {c_{ligand} = 2.0 × 10^{-3} M; M : L = 1:1; 30% (w/w) d_6-DMSO/H_2O}.

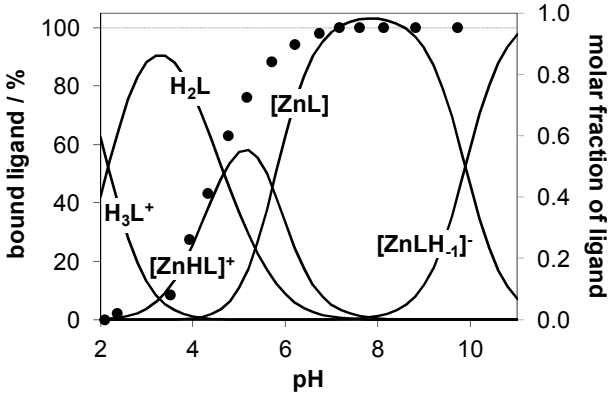

Figure 9. Concentration distribution curves for the Zn^{2+} – *L*-Pro-STSC system (solid lines) calculated on the basis of the stability constants together with the molar fraction of the bound ligand (●) estimated from the integrated area of the signals of the $C^{14}H$; $C^{4}H$; $C^{6}H$; $C^{7}H_3$, $C^{8}H_2$ protons {c_{ligand} = 2.0 × 10^{-3} M; M : L = 1:1; 30% (w/w) d_6-DMSO/H_2O}.

Due to the ability of Fe^{2+} and Fe^{3+} ions to form octahedral complexes, bis-ligand iron species could be detected as well (Table 2). In the protonated iron complexes (O^{-}, N^{1}, S) coordination mode is supposed when the non-coordinating hydrazinic N^{2} atom is protonated, and in the [ML_2] type species the ligand binds via (O^{-}, N^{1}, S^{-}) donor set based on the X-ray diffraction structures of complexes of analogous TSCs.[32–35] Species [ML_2H_{-1}] formed at basic pH are most probably mixed hydroxido species in which a coordinated donor group is displaced by an OH^{-}. UV−vis spectrophotometric titrations of the Fe^{2+} – *L*-Pro-STSC system under strictly anaerobic conditions show that the formation of the mono-ligand iron(II) species resulted in a shoulder between 430 and 480 nm, whereas formation of the green bis-ligand complexes was accompanied by the development of a wide absorption band with maximum at *ca.* 600 nm (not shown here). The absorbance values at 520 nm are increased mainly due to the formation

of the bis-ligand complexes (Figure 10). These Fe^{II} species have intense color, although their molar absorptivities are considerably lower compared to those of the α(N)-pyridyl TSC complexes.[23b,23c] In the case of the Fe^{III} complexes CT bands are found to be strongly overlapped with the ligand bands (Figure S10) and the pH-dependent UV−vis spectra indicate the predominant formation of the $[Fe(III)L_2]^-$ complex (λ_{max} = 374 nm; ε_{374nm}= 18600 $M^{-1}cm^{-1}$) between pH 6.8 and 9.8 even in a diluted solution (c = 2×10^{-5} M), as it is expected on the basis of pH-metry (Figure S10). As a consequence of the high stability of the Fe^{3+} – *L*-Pro-STSC complexes, the bis-ligand species is able to preserve its original integrity almost completely with dilution up to the micromolar concentration range at physiological pH, while the iron(II) complexes with much lower stability can dissociate to the mono-ligand species with decreasing analytical concentrations (Figure 11). Comparing the stability of the iron *L*-Pro-STSC complexes to that of the α(N)-pyridyl TSCs it can be noted that the substitution of the pyridyl moiety by the phenolic one results in an increased binding ability for Fe^{3+} and diminished for Fe^{2+} at pH 7.4, as it was found for the STSC complexes previously.[29]

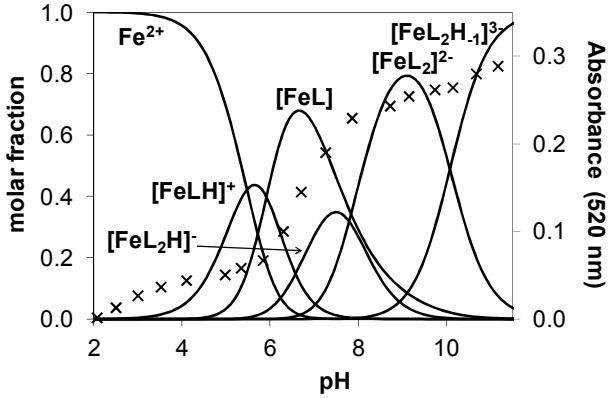

Figure 10. Concentration distribution curves for the Fe^{2+} – *L*-Pro-STSC system (solid lines) calculated on the basis of the stability constants together with the molar fraction of the absorbance values plotted against pH at 520 nm (×){c_{ligand} = 2.0×10^{-4} M; M : L = 1:2; *T* = 298 K, *I* = 0.10 M (KCl) in 30% (w/w) $DMSO/H_2O$}.

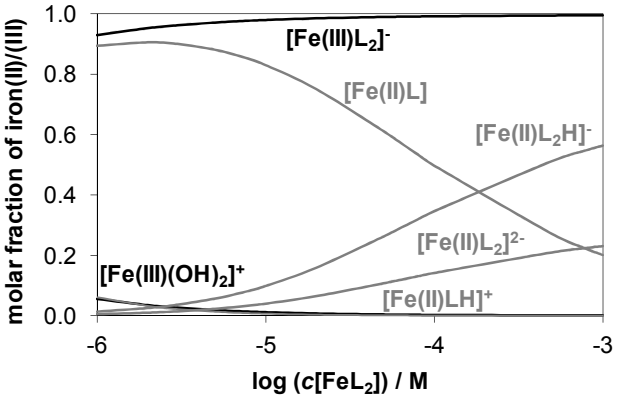

Figure 11. Representative concentration distribution diagram for the Fe^{2+} (grey lines) and Fe^{3+} (black lines) – *L*-Pro-STSC bis-ligand complexes at various total concentrations at pH 7.4 {T = 298 K; M:L = 1:2; I = 0.10 M (KCl) in 30% (w/w) DMSO/H_2O}.

As ligand *L*-Pro-STSC is strongly fluorescent at physiological pH (see above) the effect of the metal ion binding on the emission was also investigated. The metal coordination can quench the intensity but at different extent depending on metal ions (Figure S11). Fe^{3+} and Cu^{2+} quench almost completely the emission. The fluorescence is still observed in the presence of Zn^{2+} and Fe^{2+}, and might be satisfactory for monitoring the cellular distribution of these complexes by fluorescence microscopy.

Cytotoxicity in Cancer Cell Lines. The capacity of inhibiting cancer cell growth *in vitro* of compounds *L*-Pro-STSC and *D*-Pro-STSC and their corresponding copper(II) complexes was determined in human CH1 (ovarian carcinoma) and SW480 (colon carcinoma) cells by means of the colorimetric MTT assay. IC_{50} values are displayed in Table 4. Remarkably, complexation with copper(II) results in a marked increase of antiproliferative activity in both cell lines, with IC_{50} values being substantially lower than those of the ligand as well as those of a simple copper(II) salt ($CuCl_2$), indicating that cytotoxicity of the complexes cannot be explained by their potential dissociation products. The ESI mass spectra of [Cu(*L*-Pro-STSC)Cl]Cl in minimum essential medium (containing a variety of biological chelating ligands, e.g. amino acids) measured over 22 h indicate that the complex is resistant to transchelation (Figure S12). The IC_{50} values of [Cu(*L*-Pro-STSC)Cl]Cl in CH1 and SW480 are 4.6 and 5.5 μM, respectively, whereas [Cu(*D*-Pro-STSC)Cl]Cl shows IC_{50} values of 14 and 12 μM, respectively. In contrast, *L*-Pro-STSC and *D*-Pro-STSC showed a moderate cytotoxic potency with IC_{50} values of 62 and 75 μM in CH1 cells, respectively. In SW480 cells no IC_{50} value could be determined within the chosen range of concentrations up to 100

μM. Comparing IC_{50} values of *L*-Pro-STSC and *D*-Pro-STSC with those of their copper(II) complexes in CH1 cells, complexation with copper(II) hence results in a 13-fold and 5-fold increase in cytotoxicity. In both tested cell lines the ligand as well as the complex with an *L*-proline moiety led to slightly improved antiproliferative activity than the compounds with a *D*-proline moiety. Assuming that the presence of the proline moiety results in an interference with the cellular amino acid metabolism, this might reflect an influence of stereoselectivity of certain components of this metabolism, which normally deals only with the *L* isomers.

Table 4. Cytotoxicity of *L*-Pro-STSC and *D*-Pro-STSC and their copper(II) complexes compared to copper(II) chloride in two human cancer cell lines.

	IC_{50} [μM][a]	
	SW480	CH1
L-Pro-STSC	> 100	62 ± 3
[Cu(*L*-Pro-STSC)Cl]Cl	5.5 ± 0.4	4.6 ± 0.6
D-Pro-STSC	> 100	75 ± 8
[Cu(*D*-Pro-STSC)Cl]Cl	12 ± 1	14 ± 2
$CuCl_2 \cdot 2H_2O$[b]	> 160	43 ± 3

[a] 50% inhibitory concentrations in SW480 and CH1cells after exposure for 96 h in the MTT assay. Values are the mean ± standard deviation obtained from at least three independent experiments.

[b] taken from ref. 36.

Final remarks. Stability and stoichiometry of Cu^{2+}, Zn^{2+}, Fe^{2+} and Fe^{3+} complexes of *L*-Pro-STSC were determined by pH-potentiometry, and the speciation was confirmed. The most feasible coordination modes were proposed based on various spectroscopic methods (EPR, ^{1}H NMR, CD, UV−vis). Formation of mono-ligand complexes for Cu^{2+} and Zn^{2+} was found, while Fe^{2+} and Fe^{3+} ions form in addition to mono-ligand complexes bis-ligand species. In the protonated complexes the tridentate coordination mode via the (O^-, N^1, S) set with protonated non-coordinating hydrazinic N^2 atom is the most probable. (O^-, N^1, S^-) coordination mode is realized in [ML] and [ML_2] complexes, while formation of mixed hydroxido species is found at basic pH values. Complexes $[Fe(III)L_2]^-$ and [CuL] possess so high stability that their dissociation at physiological pH hardly takes place at the micromolar, the biologically more

relevant, concentration range. However, the extent of the complex dissociation in the case of the lower stability Zn^{2+} and Fe^{2+} species is significant. The complexes formed with *L*-Pro-STSC exhibit fairly similar behavior compared to STSC, the reference model compound, regarding the type, the stability and coordination mode, although, formation of somewhat higher stability Fe^{3+}-complexes is found with *L*-Pro-STSC. The effect of the side chain proline moiety is mainly manifested in the increase of the water-solubility of the ligand and its metal complexes.

Whereas the thiosemicarbazone-proline conjugates *L*-Pro-STSC and *D*-Pro-STSC show only a moderate cytotoxic potency in cancer cells, the corresponding copper(II) complexes display a tremendously increased potency. *L*-Pro-STSC as well as its copper(II) complex show slightly higher antiproliferative activity than the compounds with a *D*-Pro moiety. Studies on the impact of copper(II) coordination of proline-thiosemicarbazones on the topoisomerase IIα inhibition and the antiproliferative activity in cancer cells expressing different levels of topoisomerase IIα are underway, since the increased potency of copper(II) complexes cannot be explained by the difference in lipophilicity alone.

Experimental

Chemicals

2-Hydroxy-5-methylbenzaldehyde, thiosemicarbazide, triethylamine were purchased from Acros Organics, whereas methyl (S)-pyrrolidine-2-carboxylate hydrochloride was from VWR and methyl (R)-pyrrolidine-2-carboxylate hydrochloride from Alfa Aesar. 3-(Chloromethyl)-2-hydroxy-5-methylbenzaldehyde was synthesized according to the slightly modified published procedure.[30] Prolonged reaction time (2 h) resulted in a 15% increase of the yield. $CuCl_2$, $ZnCl_2$ and $FeCl_3$ (*puriss*, Reanal) were dissolved in known amount of HCl in order to get the Cu^{2+}, Zn^{2+} and Fe^{3+} stock solutions, respectively. Their concentrations were determined by complexometry via the EDTA complexes. The Fe^{2+} stock solution was obtained from fine Fe powder (*puriss*, Reanal) dissolved in a known amount of HCl solution under a purified, strictly oxygen-free argon atmosphere, then filtered, stored and used under anaerobic conditions. KSCN (Sigma-Aldrich) solution was used to check the absence of Fe^{3+} traces in the Fe^{2+} stock solution. The concentration of the Fe^{2+} solution was determined by permanganometric titrations under acidic conditions. Accurate strong acid content of the metal stock solutions was determined by pH-potentiometric titrations.

Synthesis of ligands

(*S*)-1. To a solution of 3-(chloromethyl)-2-hydroxy-5-methylbenzaldehyde (1.34 g, 7.25 mmol) in THF (50 mL) was added under stirring a solution of methyl (*S*)-pyrrolidine-2-carboxylate hydrochloride (1.49 g, 9.00 mmol) in CH_2Cl_2 (50 mL). Afterwards, triethylamine (2.52 mL, 18.00 mmol) in THF (25 mL) was added and stirring continued at room temperature overnight. Next day, the reaction mixture was diluted with THF (300 mL) and the precipitate of triethylammonium chloride was filtered off. The solution was freed from solvent under reduced pressure and the residue was purified by column chromatography by using as eluent ethyl acetate/hexane 3:7. The product was dried in vacuo. Yield: 1.02 g, 51%. Anal. Calcd for $C_{15}H_{19}O_4N$ (M_r 277.32 g/mol) (%): C, 64.97; H, 6.91; N, 5.05. Found: C, 64.85; H, 6.67; N, 4.98. ^{1}H NMR (DMSO-d_6, δ) 10.29 (s, 1H, HC=O), 7.38 (s, 1H, Ar), 7.26 (s, 1H, Ar), 4.08 (d, 1H, J = 13.98 Hz, CH_2), 3.68 (s, 3H, -OCH_3), 3.6 (d, 1H, J = 13.98 Hz, CH_2), 3.48–3.43 (m, 1H, Pro), 2.92–2.86 (m, 1H, Pro), 2.42–2.36 (m, 1H, Pro), 2.24 (s, 3H, CH_3) 2.22–2.16 (m, 1H, Pro), 1.91–1.70 (m, 3H, Pro). ^{13}C{^{1}H} NMR (DMSO-d_6, δ): 191.49; 174.45; 158.86; 136.73; 128.17; 127.65; 125.50; 122.40; 65.03; 55.27; 53.02; 52.41; 29.52; 23.57; 20.32. ESI-MS in MeOH (negative): *m/z* 276 $[M-H]^-$.

(*R*)-1. To a solution of 3-(chloromethyl)-2-hydroxy-5-methylbenzaldehyde (1.95 g, 10.6 mmol) in THF (50 mL) was added under stirring a solution of methyl (*R*)-pyrrolidine-2-carboxylate hydrochloride (2.51 g, 15.1 mmol) in CH_2Cl_2 (50 mL). Afterwards, triethylamine (4.5 mL, 30.0 mmol) in THF (14 mL) was added and stirring continued at room temperature overnight. Next day, the reaction mixture was diluted with THF (300 mL) and the precipitate of triethylammonium chloride was filtered off. The solution was freed from solvent and the residue was purified by column chromatography by using as eluent ethyl acetate/hexane 3:7. The product was dried in vacuo. Yield: 1.14 g, 39%. Anal. Calcd for $C_{15}H_{19}NO_4$ (M_r 277.32 g/mol) (%): C, 64.97; H, 6.91; N, 5.05. Found: C, 64.85; H, 6.67; N, 4.98. ^{1}H NMR (DMSO-d_6, δ): 10.29 (s, 1H, HC=O), 7.38 (s, 1H, Ar), 7.26 (s, 1H, Ar), 4.08 (d, 1H, J = 13.90 Hz, CH_2), 3.68 (s, 3H, -OCH_3), 3.60 (d, 1H, J = 13.90 Hz, CH_2), 3.48–3.43 (m, 1H, Pro), 2.92–2.86 (m, 1H, Pro), 2.42–2.36 (m, 1H, Pro), 2.24 (s, 3H, CH_3) 2.22–2.16 (m, 1H, Pro), 1.91–1.70 (m, 3H, Pro). ^{13}C{^{1}H} NMR (DMSO-d_6, δ): 191.45; 174.43; 158.86; 136.70; 128.15; 127.61; 125.48; 122.39; 65.01; 55.28; 53.00; 52.39; 29.51; 23.56; 20.30. ESI-MS in MeOH (negative): *m/z* 276 $[M-H]^-$. ESI-MS in MeOH (positive): *m/z* 278 $[M+H]^+$.

2-Hydroxy-3-methyl-(*S*)-pyrrolidine-2-carboxylate-5-methylbenzaldehyde thiosemicarbazone (*L*-Pro-STSC). To a warm solution of the (*S*)-**1** (1.14 g, 4.10 mmol) in ethanol (30 mL) was added a solution of thiosemicarbazide (0.46 g, 5.00 mmol) in hot water (30 mL). The reaction mixture was heated at 70−75°C with continuous stirring for 75 h. After cooling to room temperature chloroform (100 mL) was added. The aqueous phase was separated and allowed to stand at 5 °C overnight. The white precipitate was filtered off, washed with water, ethanol, chloroform and dried in vacuo. Yield: 0.56 g, 41%. Anal. Calcd for $C_{15}H_{20}N_4O_3S{\cdot}1.5H_2O$ (M_r 363.4 g/mol) (%): C, 49.57; H, 6.38; N, 15.42; S, 8.82. Found: C, 49.62; H, 6.37; N, 15.51; S, 9.07. ^{1}H NMR (DMSO-d$_6$, δ): 11.41 (s, 1H, N^{2}H); 8.39 (s, 1H, HC^{14}=N^2); 8.11 (s, 1H, N^{3}H$_2$); 7.91 (s, 1H, N^{3}H$_2$); 7.75 (s, 1H, C^{4}H); 6.95 (s, 1H, C^{6}H); 4.14 (d, 1H (*J* = 13.52 Hz), C^{8}H); 3.49 (d, 1H (*J* = 13.52 Hz), C^{8}H); 3.39–3.37 (m, 1H, C^{9}H); 2.93–2.84 (m, 1H, C^{12}H); 2.45–2.36 (m, 1H, C^{12}H); 2.27–2.23 (m, 1H, C^{10}H); 2.21 (s, 3H, C^{7}H$_3$); 1.91–1.78 (m, 2H, C^{10}H, C^{11}H); 1.77–1.66 (m, 1H, C^{11}H). ^{13}C{^{1}H} NMR (DMSO-d$_6$, δ): 178.11; 174.94; 154.60; 139.61; 131.83; 127.79; 126.11; 123.46; 120.61; 65.59; 56.39; 53.04; 29.46; 23.46; 20.5. ESI-MS in MeOH (positive): *m*/*z* 359 $[H_2L+Na]^+$; 337 $[H_2L+H]^+$.

2-Hydroxy-3-methyl-(*R*)-pyrrolidine-2-carboxylate-5-methylbenzaldehyde thiosemicarbazone (*D*-Pro-STSC). To a warm solution of (*R*)-**1** (2.05 g; 7.40 mmol) in ethanol (30 mL) was added a solution of thiosemicarbazide (0.78 g, 8.50 mmol) in hot water (30 mL). The reaction mixture was heated at 70−75°C with continuous stirring for 12 h. After cooling to room temperature chloroform (100 mL) was added. The aqueous phase was separated and allowed to stand at 5 °C overnight. The white precipitate was filtered off, washed with water, ethanol, chloroform and dried in vacuo. Yield: 0.45 g, 18%. Anal. Calcd for $C_{15}H_{20}N_4O_3S{\cdot}H_2O$ (M_r 354.43 g/mol) (%): C, 50.83; H, 6.26; N, 15.81; S, 9.05. Found: C, 51.05; H, 6.21; N, 15.84; S, 9.20. ^{1}H NMR (DMSO-d6, δ): 11.41 (s, 1H, NH); 8.39 (s, 1H, HC=N); 8.11 (s, 1H, NH_2); 7.91 (s, 1H, NH_2); 7.75 (s, 1H, Ar); 6.95 (s, 1H, Ar); 4.14 (d, 1H (*J* = 13.52 Hz), CH_2); 3.50 (d, 1H (*J* = 13.52 Hz), CH_2); 3.39–3.37 (m, 1H, Pro, overlapped water peak); 2.93–2.84 (m, 1H, Pro); 2.45–2.36 (m, 1H, Pro); 2.27–2.23 (m, 4H, Pro, CH_3); 1.91–1.78 (m, 2H, Pro); 1.77–1.66 (m, 1H, Pro). ^{13}C{^{1}H} NMR (DMSO-d$_6$, δ): 178.12; 174.92; 154.60; 139.63; 131.84; 127.8; 126.14; 123.44; 120.61; 65.59; 56.37; 53.04; 29.46; 23.45; 20.5. ESI-MS in MeOH (positive): *m*/*z* 359 $[H_2L+Na]^+$; 337 $[H_2L+H]^+$.

Synthesis of copper(II) complexes

[Cu(*S*-H_2L)Cl]Cl. To a solution of *L*-Pro-STSC (0.04 g, 0.12 mmol) in methanol (50 mL) was added a solution of $CuCl_2 \cdot 2H_2O$ (0.04 g, 0.26 mmol) in methanol (3 mL) and the reaction mixture was refluxed for 1 h. After cooling to room temperature the solution was evaporated under reduced pressure to about 5 mL. The green crystalline product was obtained by slow vapor diffusion of diethylether into the concentrated methanolic solution. The product was washed with diethylether/methanol 5:1 (5 mL) and dried in vacuo overnight. Yield: 0.03 g; 55.4%. Anal. Calcd for $CuC_{15}H_{20}N_4O_3SCl_2 \cdot 0.4CH_3OH$ (M_r 483.68 g/mol) (%): C, 38.24; H, 4.5; N, 11.58; S, 6.63. Found: C, 38.05; H, 4.45; N, 11.23; S, 6.48. ESI-MS in MeOH (positive): *m*/*z* 398 $[Cu^{II}(HL)]^+$. ESI-MS in MeOH (negative): *m*/*z* 396 $[Cu^{II}(L-H)]^-$; *m*/*z* 432 $[Cu^{II}(L)Cl]^-$.

[Cu(*R*-H_2L)Cl]Cl. To a solution of *D*-Pro-STSC (0.04 g, 0.12 mmol) in methanol (50 mL) was added a solution of $CuCl_2 \cdot 2H_2O$ (0.04 g, 0.26 mmol) in methanol (3 mL) and the reaction mixture was refluxed for 1 h. After cooling to room temperature the solution was evaporated under reduced pressure to about 5 mL. The green crystalline product was obtained by slow vapor diffusion of diethylether into the concentrated methanolic solution. The product was washed with diethylether/methanol 5:1 (5 mL) and dried in vacuo overnight. Yield: 0.05 g, 83.9%. Anal. Calcd for $CuC_{15}H_{20}N_4O_3SCl_2 \cdot 0.3CH_3OH$ (M_r 480.47 g/mol) (%): C, 38.25; H, 4.45; N, 11.66; S, 6.67. Found: C, 37.95; H, 4.35; N, 11.28; S, 6.58. ESI-MS in MeOH (positive): *m*/*z* 398 $[Cu^{II}(HL)]^+$. ESI-MS in MeOH (negative): *m*/*z* 396 $[Cu^{II}(L-H)]^-$; *m*/*z* 432 $[Cu^{II}(L)Cl]^-$.

pH-potentiometric measurements. The purity and aqueous phase stability of the ligand *L*-Pro-STSC was verified and the exact concentrations of the stock solutions prepared were determined by the Gran method.[37]

The pH-metric measurements for determination of the protonation constants of the ligand and the overall stability constants of the metal complexes were carried out at 25.0 ± 0.1 ^oC in DMSO/water 30:70 (w/w) as solvent and at an ionic strength of 0.10 M (KCl, Sigma-Aldrich) in order to keep the activity coefficients constant. (In previous studies on STSC and α(N)-pyridyl TSCs 30% (w/w) DMSO/H_2O solvent mixture was used.[23b,23c,29] In order to obtain comparable data the same conditions were applied, although the presence of only 20% (w/w) DMSO is found to be sufficient for dissolution of *L*-Pro-STSC at the concentration levels necessary for pH-potentiometric titrations, i.e. ≥1−2 mM.) The titrations were performed with

carbonate-free KOH solution of known concentration (0.10 M). Both the base and the HCl were Sigma-Aldrich products and their concentrations were determined by pH-potentiometric titrations. An Orion 710A pH-meter equipped with a Metrohm combined electrode (type 6.0234.100) and a Metrohm 665 Dosimat burette were used for the pH-metric measurements. The electrode system was calibrated to the pH = log[H^+] scale in the DMSO/water solvent mixture by means of blank titrations (strong acid vs strong base; HCl vs KOH), similarly to the method suggested by Irving *et al.*[38] in pure aqueous solutions. The average water ionization constant, pK_w, is 14.52 ± 0.05 with DMSO/water 30:70 (w/w) as solvent at 25 °C, which corresponds well to the literature data.[23b,23c,39] The reproducibility of the titration points included in the calculations was within 0.005 pH. The pH-metric titrations were performed in the pH range 2.0 – 12.5. The initial volume of the samples was 10.0 mL. The ligand concentration was in the range $2–3 \times 10^{-3}$ M and metal ion-to-ligand ratios of 1:1 – 1:4 were used. The accepted fitting of the titration curves was always less than 0.01 mL. Samples were deoxygenated by bubbling purified argon through them for *ca.* 10 min prior to the measurements. In the case of Fe^{2+} samples, argon overpressure was used when Fe^{2+} was added to the samples in tightly closed vessels, which were prior completely deoxygenated by bubbling a stream of purified argon through them for *ca.* 20 min. Argon was also passed over the solutions during the titrations.

The protonation constants of the ligands were determined with the computer program SUPERQUAD.[40] PSEQUAD[41] was utilized to establish the stoichiometry of the complexes and to calculate the stability constants ($\log\beta\square M_pL_qH_r\square$) from the literature data for Fe^{III} hydroxido complexes.[42] $\beta\square M_pL_qH_r\square$ is defined for the general equilibrium pM + qL + rH $\rightleftharpoons$ $M_pL_qH_r$ as $\beta(M_pL_qH_r) = [M_pL_qH_r]/[M]^p[L]^q[H]^r$ where M denotes the metal ion and L the completely deprotonated ligand (see SI for details). The calculations were always made from the experimental titration data measured in the absence of any precipitate in solution.

UV–vis spectrophotometric, spectrofluorimetric, CD and ^{1}H NMR measurements. A Hewlett Packard 8452A diode array spectrophotometer was used to record the UV–vis spectra in the interval 260 – 820 nm. The path length was 1 cm. Protonation and stability constants and the individual spectra of the species were calculated by the computer program PSEQUAD.[41] The spectrophotometric titrations were performed on samples of the *L*-Pro-STSC alone or with Cu^{2+}, Fe^{3+} or Fe^{2+} ions; the concentration of the ligand was 4×10^{-5} M

(for the ligand and Fe^{3+} containing samples), 2×10^{-4} M (for Fe^{2+} containing samples) or 2×10^{-3} M (for Cu^{2+} containing samples) and the metal-to-ligand ratios were 0:1, 1:1 and 1:2 over the pH range between 2 and 12 at an ionic strength of 0.10 M (KCl) in 30% (w/w) DMSO/H_2O at 25.0 ± 0.1 ^oC. For Fe^{2+} samples, spectra were recorded under strictly anaerobic conditions. Measurements for Fe^{3+} − *L*-Pro-STSC system at metal-to-ligand ratio 1:1 were also carried out by preparing individual samples in which the 0.1 M KCl was partially or completely replaced by HCl and pH values, varying in the range *ca.* 1.0 – 1.8, were calculated from the HCl content. For the calculation of the stability constants of the protonated mono-ligand Fe^{3+} – *L*-Pro-STSC complex mainly CT bands (which are strongly overlapped with the ligand bands) were used (λ = 300 − 470 nm).

The pH-dependent fluorescence measurements were carried out on a Hitachi-4500 spectrofluorimeter with the excitation at 393 nm. The emission spectra were recorded using 5 nm/5 nm slit widths in 1 cm quartz cell in the pH range between 2 and 12 in 30% (w/w) DMSO/H_2O at 25.0 ± 0.1 ^oC. Samples contained 5×10^{-6} M *L*-Pro-STSC ligand alone or with 5×10^{-6} M Cu^{2+} or Zn^{2+} ions or 2.5×10^{-6} M Fe^{2+} at 0.1 M (KCl) ionic strength. Three-dimensional spectra were recorded at 230 – 500 nm excitations and at 240 – 600 nm emission wavelengths for the 5×10^{-6} M ligand containing samples at pH 5.1; 7.6 and 10.0 using 2.5 nm/2.5 nm slit widths.

^1H NMR studies were carried out on a Bruker Ultrashield 500 Plus instrument. *L*-Pro-STSC was dissolved in a 30% (w/w) d_6-DMSO/H_2O mixture in a concentration of 2×10^{-3} M and the Zn^{2+}-to-ligand ratios were 0:1 and 1:1. The direct pH-meter readings were corrected according to method of Irving *et al*.[38]

CD spectra were recorded on a Jasco J-815 spectrometer in an optical cell of 1.0 cm path length. The analytical concentration of *D* or *L*-Pro-STSC ligands or the Cu^{2+}-*D* or *L*-Pro-STSC complexes was 6.5×10^{-5} M at pH 7.4 in pure aqueous solution and spectra were recorded in the wavelength interval from 215 to 500 nm. 2.0×10^{-3} M ligand concentration was used for the Cu^{2+} − *L*-Pro-STSC system at 1:1 metal-to-ligand ratio in a 30% (w/w) DMSO/H_2O mixture and pH was varied between 2 and 12 and spectra were analyzed in the range of 460 − 700 nm. CD data are given as the differences in molar absorptivities between left and right circularly polarized light, based on the concentration of the ligand ($\Delta\varepsilon = \Delta A / l / c_{\text{ligand or complex}}$).

Determination of the distribution coefficient (*D*). *D* values of *L*- and *D*-Pro-STSC and their copper(II) complexes were determined by the traditional shake flask method in *n*-octanol/buffered aqueous solution at pH 7.4 (4-(2-hydroxyethyl)-1-piperazineethanesulfonic acid, HEPES) at 25.0±0.2 ^{o}C as described previously.[29] Two parallel experiments were performed for each sample. The ligands were dissolved at 4×10^{-5} M and the complexes in 6.4×10^{-5} M in the *n*-octanol pre-saturated aqueous solution of the buffer (0.01 M) at constant ionic strength (0.10 M KCl). The aqueous solutions and *n*-octanol with 1:1 phase ratio were gently mixed with 360° vertical rotation for 3 h to avoid the emulsion formation, and the mixtures were centrifuged at 5000 rpm for 3 min by a temperature controlled centrifuge (Sanyo) at 25 ^{o}C. After separation UV–vis spectra of the ligands or complexes in the aqueous phase were compared to those of the original aqueous solutions and $D_{7.4}$ value was calculated as the mean of (Absorbance (original solution) / Absorbance (aqueous phase after separation) – 1) obtained at the region of λ_{max} ± 10 nm values.

EPR measurements and deconvolution of the spectra. All CW-EPR spectra were recorded with a BRUKER EleXsys E500 spectrometer (microwave frequency 9.81 GHz, microwave power 10 mW, modulation amplitude 5 G, modulation frequency 100 kHz). During titration, the isotropic EPR spectra were recorded at room temperature in a circulating system. Eleven and ten EPR spectra were recorded for samples with 1:1 and 1:2 Cu^{2+}-to-ligand ratios, respectively at 2.0×10^{-3} M *L*-Pro-STSC concentration between pH 2.4 − 12 in 30% (w/w) DMSO/H_2O at I = 0.10 M (KCl). KOH solution was added to the stock solution to change the pH which was measured with a Radiometer PHM240 pH/ion Meter equipped with a Metrohm 6.0234.100 glass electrode. A Heidolph Pumpdrive 5101 peristaltic pump was used to circulate the solution from the titration pot through a capillary tube into the cavity of the instrument. The titrations were carried out under argon atmosphere. At various pH values, samples of 0.10 mL were taken, and frozen in liquid nitrogen, and the CW-EPR spectra were recorded under the same instrumental conditions as the room-temperature spectra described above.

The series of room-temperature CW-EPR spectra were simulated simultaneously by the „two-dimensional" method using the 2D_EPR program.[43] Each component curve was described by the isotropic EPR parameters g_o, A_o^{Cu} copper hyperfine and A_o^{N} nitrogen hyperfine couplings, and the relaxation parameters α, β, γ which define the line widths in the equation

$\sigma_{MI}=\alpha+\beta M_I+\gamma M_I^2$, where M_I denotes the magnetic quantum number of copper nucleus. The concentrations of the complexes were varied by fitting their formation constants β□□$M_pL_qH_r$) defined by the general equilibrium found in the pH-potentiometric studies section.

For each spectrum, the noise-corrected regression parameter (R_j for the j^{th} spectrum) is derived from the average square deviation (SQD) between the experimental and the calculated intensities. For the series of spectra, the fit is characterized by the overall regression coefficient R, calculated from the overall average SQD. The details of the statistical analysis were published previously.[44]

The anisotropic spectra were analyzed individually with the EPR program,[44] which gives the anisotropic EPR parameters (g_x, g_y, g_z, A_x^{Cu}, A_y^{Cu}, A_z^{Cu}, A_x^N, A_y^N, A_z^N, and the orientation dependent line width parameters). Since a natural $CuCl_2$ was used for the measurements, the spectra were calculated as the sum of the spectra of ^{63}Cu and ^{65}Cu weighted by their natural abundances. The quality of fit was characterized by the noise-corrected regression parameter R_j as above. The copper and nitrogen coupling constants and the relaxation parameters were obtained in field units (Gauss = 10^{-4} T).

Crystallographic Structure Determination. X-ray diffraction measurement was performed on a Bruker X8 APEXII CCD diffractometer. A single crystal of [Cu(*R*-H_2L)Cl]Cl was positioned at 40 mm from the detector, and 1138 frames were measured, each for 60 s over 1° scan width. The data was processed using SAINT software.[45] Crystal data, data collection parameters, and structure refinement details are given in Table 5. The structure was solved by direct methods and refined by full-matrix least-squares techniques. Non-H atoms were refined with anisotropic displacement parameters. H atoms were inserted in calculated positions and refined with a riding model. The five-membered proline ring in both crystallographically independent complex cations (A and B) of [Cu(*R*-H_2L)Cl]Cl was found to be disordered over two positions with s.o.f. 0.50:0.50. In addition, one oxygen atom of the −COOH group in complex cation B is also disordered over two positions, each with 50% occupancy. The disorder was resolved with restraints on displacement parameters and on bond distances using DELU and SADI instructions of SHELX-97, respectively. The following software programs and computer were used: structure solution, *SHELXS-97*; refinement, *SHELXL-97*;[46] molecular diagrams, *ORTEP-3*;[47] computer, Intel CoreDuo.

Table 5. Crystal data and details of data collection for [Cu(*R*-H_2L)Cl]Cl.

Compound	[Cu(*R*-H_2L)Cl]Cl
Empirical formula	$C_{15}H_{20}Cl_2CuN_4O_3S$
Fw	470.85
Space group	$P2_1$
a [Å]	7.3130(3)
b [Å]	21.8734(8)
c [Å]	11.7535(5)
β [°]	99.423(2)
V [Å^3]	1854.72(13)
Z	4
λ [Å]	0.71073
ρ_{calcd} [g cm^{-3}]	1.686
Crystal size [mm^3]	0.16 × 0.05 × 0.03
T [K]	120(2)
μ [mm^{-1}]	1.602
R_1[a]	0.0356
wR_2[b]	0.0795
GOF[c]	1.014

[a] $R_1 = \Sigma||F_o| - |F_c||/\Sigma|F_o|$. [b] $wR_2 = \{\Sigma[w(F_o^2 - F_c^2)^2]/\Sigma[w(F_o^2)^2]\}^{1/2}$. [c] GOF = $\{\Sigma[w(F_o^2 - F_c^2)^2]/(n-p)\}^{1/2}$, where n is the number of reflections and p is the total number of parameters refined.

Cell lines and Culture Conditions. Human CH1 (ovarian carcinoma) and SW480 (colon carcinoma) cells were kindly provided by Lloyd R. Kelland (CRC Centre for Cancer Therapeutics, Institute of Cancer Research, Sutton, UK) and Brigitte Marian (Institute of Cancer Research, Department of Medicine I, Medical University of Vienna, Austria), respectively. Cells were grown in 75 cm² culture flasks (CytoOne/Starlabs, Germany) as adherent monolayer cultures in Minimal Essential Medium (MEM) supplemented with 10% heat-inactivated fetal bovine serum, 1 mM sodium pyruvate, 4 mM *L*-glutamine and 1% non-essential amino acids (from 100× ready-to-use stock) (all purchased from Sigma-Aldrich, Vienna, Austria). Cultures were maintained at 37 °C in a humidified atmosphere containing 5% CO_2.

Cytotoxicity Tests in Cancer Cell Lines. Antiproliferative effects were determined by means of a colorimetric microculture assay (MTT assay, MTT = 3-(4,5-dimethyl-2-thiazolyl)-2,5-diphenyl-2H-tetrazolium bromide). Cells were harvested from culture flasks by

trypsinization and seeded in 100 µL aliquots into 96-well microculture plates (CytoOne/Starlabs, Germany) in densities of 2×10^3 cells/well (SW480) and 1×10^3 cells/well (CH1), in order to ensure exponential growth of untreated controls throughout the experiment. After a 24 h pre-incubation, dilutions of the test compounds in 100 µL/well complete culture medium were added. Because of low aqueous solubility, the test compounds were dissolved in DMSO first and then serially diluted in complete culture medium such that the effective DMSO content did not exceed 0.5%. After exposure for 96 h, all media were replaced by 100 µL/well RPMI 1640 medium (supplemented with 10% heat-inactivated fetal bovine serum and 2 mM *L*-glutamine) plus 20 µL/well MTT solution in phosphate-buffered saline (5 mg/ml). After incubation for 4 h, the medium/MTT mixtures were removed, and the formazan crystals formed by viable cells were dissolved in 150 µL DMSO per well. Optical densities at 550 nm were measured with a microplate reader (Biotek ELx808), using a reference wavelength of 690 nm to correct for unspecific absorption. The quantity of vital cells was expressed in terms of T/C values by comparison to untreated control microcultures, and 50% inhibitory concentrations (IC_{50}) were calculated from concentration-effect curves by interpolation. Evaluation is based on means from at least three independent experiments, each comprising three microcultures per concentration level.

Acknowledgments

This work has been supported by the Austrian Science Fund (Project number P19629-N19), Hungarian Research Foundation OTKA K77833, K72781, the Hungarian-Austrian Action Foundation and „TÁMOP-4.2.1/B-09/1/KONV-2010-0005. É.A.E. gratefully acknowledges the financial support of Bolyai J. research fellowships. We thank Alexander Roller for collection of X-ray data.

Supporting information available: CD and UV−vis spectra of *L*-Pro-STSC and *D*-Pro-STSC (Figure S1), unit cell and hydrogen bonding interactions for [Cu(*R*-Pro-STSC)Cl]Cl (Figure S2), stack formation in the crystal structure of [Cu(*R*-Pro-STSC)Cl]Cl (Figure S3), calculated UV−vis spectra of the individual species of *L*-Pro-STSC (Figure S4), pH-dependent ^{1}H NMR spectra of *L*-Pro-STSC (Figure S5), log$D_{7.4}$ determination for *L*-Pro-STSC by UV−vis spectroscopy (Figure S6), log$D_{7.4}$ determination for [Cu(*L*-Pro-STSC)Cl]Cl by UV−vis spectroscopy (Figure S7), experimental and simulated EPR spectra of Cu^{2+}− *L*-Pro-STSC system (Figure S8), ^{1}H NMR spectra of *L*-Pro-STSC at pH 9.8 and Zn^{2+}− *L*-Pro-STSC system at pH 8.1 and 9.7 (Figure S9), pH-dependent UV−vis spectra of the Fe^{3+}−*L*-

Pro-STSC system and the corresponding concentration distribution curves (Figure S10), fluorescence intensity of emission at 498 nm for the *L*-Pro-STSC and 1:1 mixtures of Zn^{2+}, Fe^{2+} and Cu^{2+} with *L*-Pro-STSC (Figure S11), ESI MS spectra of [Cu(*L*-Pro-STSC)Cl]Cl in MEM (Figure S12), definition of the stability constants of the metal complexes; crystallographic data for [Cu(*R*-Pro-STSC)Cl]Cl in CIF format. This material is available free of charge via the Internet at http://pubs.acs.org.

References

(1) (a) West, D. X.; Padhye, S. B.; Sonawane, P. B. *Struct. Bond.* **1991**, *76*, 1−50 ; (b) Casas, J. S.; Garcia-Tasende, M. S.; Sordo, J. *Coord. Chem. Rev.* **2000**, *209*, 197−261.

(2) (a) Knox, J. J.; Hotte, S. J.; Kollmannsberger, C.; Winquist, E.; Fisher, B.; Eisenhauer, E. A. *Invest. New Drugs* **2007**, *25*, 471−477; (b) Stringer, T.; Chellan, P.; Therrien, B.; Shunmoogam-Gounden, N.; Hendricks, D. T.; Smith, G. S. *Polyhedron* **2009**, *28*, 2839−2846; (c) Stringer, T.; Hendricks, D. T.; Guzgay, H.; Smith, G. S. *Polyhedron* **2012**, *31*, 486−493.

(3) Easmon, J.; Heinisch, G.; Holzer, W.; Rosenwirth, B. *J. Med. Chem.* **1992**, *35*, 3288−3296.

(4) Klayman, D. L.; Bartosevich, J. F.; Griffin, T. S.; Mason, C. J.; Scovill, J. P. *J. Med. Chem.* **1979**, *22*, 855−862.

(5) Ma, B.; Goh, B.C.; Tan, E. H.; Lam, K. C.; Soo, R.; Leong, S. S.; Wang, L. Z.; Mo, F.; Chan, A. T. C.; Zee, B.; Mok, T. *Invest. New Drugs* **2008**, *26*, 169−173.

(6) Karp, J. E.; Giles, F. J.; Gojo, I.; Morris, L.; Greer, J.; Johnson, B.; Thein, M.; Sznol, M.; Low, J. *Leuk. Res.* **2008**, *32*, 71−77.

(7) Mackenzie, M. J.; Saltman, D.; Hirte, H.; Low, J.; Johnson, C.; Pond, G.; Moore, M. J. *Invest. New Drugs* **2007**, *25*, 553−558.

(8) Chao, J.; Synold, T. W.; Morgan, R. J., Jr.; Kunos, C.; Longmate, J.; Lenz, J.-J.; Lim, D.; Shibata, S.; Chung, V.; Stoller, R. G.; Belani, C. P.; Gandara, D. R.; McNamara, M.; Gitlitz, B. J.; Lau, D. H.; Ramalingam, S. S.; Davies, A.; Espinoza-Delgado, I.; Newman, E. M.; Yen, Y. *Cancer. Chemother. Pharmacol.* **2012**, *69*, 835−843.

(9) Yu, Y.; Wong, J.; Lovejoy, D. B.; Kalinowski, D. S.; Richardson, D. R. *Clin. Cancer Res.* **2006**, *12*, 6876−6883.

(10) Moore, E. M.; Zedeck, M. S.; Agrawal, K. C.; Sartorelli, A. C. *Biochemistry* **1970**, *9*, 4492−4498.

(11) Kolberg, M.; Strand, K. R.; Graff, P.; Andersson, K. K. *Biochim. Biophys. Acta* **2004**, *1699*, 1−34.

(12) French, F. A.; Blanz Jr., E. J. *J. Med. Chem.* **1974**, *17*, 172−181.

(13) Moore, E.; Sartorelli, A. C. *Pharmacol. Ther.* **1984**, *24*, 439−447.

(14) Finch, R. A.; Liu, M.; Cory, A. H.; Cory, J. G.; Sartorelli, A. C. *Adv. Enzyme Regul.* **1999**, *39*, 3−12.

(15) (a) Easmon, J.; Puerstinger, G.; Heinisch, G.; Roth, T. *J. Med. Chem.* **2001**, *44*, 2164−2171; (b) Miller, M. C.; Stineman, N. C.; Vance, R. J.; West, D. X.; Hall, H. I. *Anticancer Res.* **1998**, *18*, 4131−4139.

(16) Huang, H.; Chen, W.; Ku, X.; Meng, L.; Lin, L.; Wang, X.; Zhu, C.; Wang, Y.; Chen, Z.; Li, M.; Jiang, H.; Chen, K.; Ding, J.; Liu, H. *J. Med. Chem.* 2010, *53*, 3048−3064.

(17) Zeglis, B. M.; Divilov, V.; Lewis, J. S. *J. Med. Chem.* **2011**, *54*, 2391−2398.

(18) Kowol, C. R.; Heffeter, P.; Miklos, W.; Gille, L.; Trondl, R.; Cappellacci, L.; Berger, W.; Keppler, B. K. *J. Biol. Inorg. Chem.* **2012**, *17*, 409–423.

(19) Shao, J.; Zhou, B.; Di Bilio, A. J., Zhu, L.; Wang, T.; Qi, C.; Shih, J.; Yen, Y. *Mol. Cancer Ther*. **2006**, *5*, 586−592.

(20) Chaston, T. B.; Lovejoy, D. B.; Watts, R. N.; Richardson, D. R. *Clin. Cancer Res.* **2003**, *9*, 402−414.

(21) Popović-Bijelić, A.; Kowol, C. R.; Lind, M. E. S.; Luo, J.; Enyedy, E. A.; Arion, V. B.; Gräslund, A. *J. Inorg. Biochem.* **2011**, *105*, 1422−1431.

(22) (a) Richardson, D. R.; Sharpe, P. C.; Lovejoy, D. B.; Senaratne, D.; Kalinowski, D. S.; Islam, M.; Bernhardt, P. V. *J. Med. Chem*. **2006**, *49*, 6510−6521; (b) Opletalova, V.; Kalinowski, D. S.; Vejsova, M.; Kunes, J.; Pour, M.; Jampilek, J.; Buchta, V.; Richardson, D. R. *Chem. Res. Toxicol.* **2008**, *21*, 1878−1889; (c) Jansson, P. J.; Sharpe, P. C.; Bernhardt, P. V.; Richardson, D. R. *J. Med. Chem.* **2010**, *53*, 5759−5769; (d) Kalinowski, D. S.; Yu, Y.; Sharpe, P. C.; Bernhardt, P. V.; Richardson, D. R. *J. Med. Chem.* **2007**, *50*, 3716−3729; (e) Richardson, D. R.; Kalinowski, D. S.; Richardson, V.; Sharpe, P. C.; Lovejoy, D. B.; Islam, M.; Bernhardt, P. J. *J. Med. Chem.* **2009**, *52*, 1459−1470; (f) Kowol, C. R.; Berger, R.; Eichinger, R.; Roller, A.; Jakupec, M. A.; Schmidt, P. P.; Arion, V. B.; Keppler, B. K. *J. Med. Chem.* **2007**, *50*, 1254−1265.

(23) (a) Knight, J. M.; Whelan, H.; Petering, D. H. *J. Inorg. Biochem*. **1979**, *11*, 327−338; (b) Enyedy, E. A.; Nagy, N. V.; Zsigó, E.; Kowol, C. R.; Arion, V. B.; Keppler, B. K.; Kiss, T. *Eur. J. Inorg. Chem.* **2010**, 1717−1728; (c) Enyedy, E. A.; Primik, M. F.; Kowol, C. R.; Arion, V. B.; Kiss, T.; Keppler, B. K. *Dalton Trans.* **2011**, *40*, 5895−5905.

(24) (a) Ryabova, N. A.; Ponomarev, V. I.; Zelentsov, V. V.; Atovmyan, L. O. *Kristallografiya* **1981**, *26*, 101−108; (b) Ryabova, N. A.; Ponomarev, V. I.; Zelentsov, V. V.; Atovmyan, L. O. *Kristallografiya* **1982**, *27*, 81−91; (c) Schulte, G.; Luo, X.-L.; Crabtree, R. H.; Zimmer, M. *Angew. Chem. Int. Ed.* 1991, *30*, 193−194; (d) Argay, G.; Kalman, A.; Leovac, V. M.; Cesljevic, V. I.; Ribar, B. *J. Coord. Chem.* **1996**, *37*, 165−171; (e) Soriano-Garcia, M.; Valdes-Martinez, J.; Toscano, R. A.; Gomez-Lara, J. *Acta Crystallogr.* **1985**, *C41*, 500−502.

(25) Belicchi Ferrari, M.; Capacchi, S.; Pelosi, G.; Reffo, G.; Tarasconi, P.; Albertini, R.; Pinelli, S.; Lunghi, P. *Inorg. Chim. Acta* **1999**, *286*, 134−141.

(26) Đilović, I.; Rubčić, M.; Vrdoljak, V.; Kraljević Pavelić, S.; Kralj, M.; Piantanida, I.; Cindrić, M. *Bioorg. Med. Chem*. **2008**, *16*, 5189−5198.

(27) (a) Kowol, C. R.; Eichinger, R.; Jakupec, M. A.; Galanski, M.; Arion, V. B.; Keppler, B. K. *J. Inorg. Biochem.* **2007**, *101*, 1946−1957; (b) Arion, V. B.; Jakupec, M. A.; Galanski, M.; Unfried, P.; Keppler, B. K. *J. Inorg. Biochem.* **2002**, *91*, 298−305.

(28) Sen, S.; Shit, S.; Mitra, S.; Batten, S. R. *Struct. Chem.* **2008**, *19*, 137−142.

(29) Enyedy, E. A.; Zsigo, E.; Nagy, N. V.; Kowol, C. R.; Roller, A.; Keppler, B. K.; Kiss, T. *Eur. J. Inorg. Chem*. DOI: 10.1002/ejic.201200360.

(30) (a) Wang, Q.; Wilson, C.; Blake, J. A.; Collinson, R. S.; Tasker, A. P.; Schröder, M. *Tetrahedron Lett.* **2006**, *47*, 8983−8987; (b) Huisman, M.; Koval, I. A.; Gamez, P.; Reedijk, J. *Inorg. Chim. Acta* **2006,** *359*, 1786-1794

(31) (a) Lee, W. Y.; Lee, P. P. F.; Yan, Y. K.; Lau, M. *Metallomics* **2010**, *2*, 694−705; (b)

Lee, W. Y.; Yan, Y. K.; Lee, P. P. F.; Tan, S. J.; Lim, K. H. *Metallomics* **2012**, *4*, 188−196.

(32) Wu, W. S.; Feng, Y.-L. *Z. Kristallorg.* **2003**, *218*, 529−530.

(33) Ryabova, N. A.; Ponomarev, V. I.; Atovmyan, L. O.; Zelentsov, V. V.; Shipilov, V. I. *Coord. Chem*. **1978**, *37*, 119−129.

(34) Ryabova, N. A.; Ponomarev, V. I.; Zelentsov, V. V.; Atovmyan, L. O. *Kristallografiya* **1982**, *27*, 279−287.

(35) Floquet, S.; Guillou, N.; Negrier, P.; Riviere, E.; Boillot, M. L. *New J. Chem.* **2006**, *30*, 1621−1627.

(36) Primik, M. F.; Mühlgassner G.; Jakupec M. A.; Zava O.; Dyson P. J.; Arion V. B.; Keppler B. K, *Inorg. Chem.*, **2010**, *49*, 302−311.

(37) Gran, G. *Acta Chem. Scand.* **1950**, *4*, 559−577.

(38) Irving, H. M.; Miles, M. G.; Pettit, L. D. *Anal. Chim. Acta* **1967**, *38*, 475−488.

(39) SCQuery, The IUPAC Stability Constants Database, Academic Software (Version 5.5), Royal Society of Chemistry, 1993–2005.

(40) Sabatini, A.; Vacca, A.; Gans, P. *Talanta* **1974**, *21*, 53–77.

(41) Zékány, L.; Nagypál, I. in: Computational Methods for the Determination of Stability Constants (Ed.: D. L. Leggett), Plenum Press, New York, 1985, p. 291–353.

(42) Baes, C.F.; Mesmer, R. E. The Hydrolysis of Cations, Wiley, New York, 1976.

(43) Rockenbauer, A.; Szabó-Plánka, T.; Arkowi, Zs.; Korecz, L. *J. Am. Chem. Soc.* **2001**, *123*, 7646−7654.

(44) Rockenbauer, A.; Korecz, L. *Appl. Magn. Reson.* **1996**, *10*, 29−43.

(45) *SAINT-Plus*, version 7.06a and APEX2; Bruker-Nonius AXS Inc.: Madison, WI, 2004.

(46) Sheldrick, G. M. *Acta Crystallogr.* **2008**, *A46*, 112–122.

(47) Johnson, G. K. Report ORNL-5138; OAK Ridge National Laboratory; Oak Ridge, TN, 1976.

Synopsis

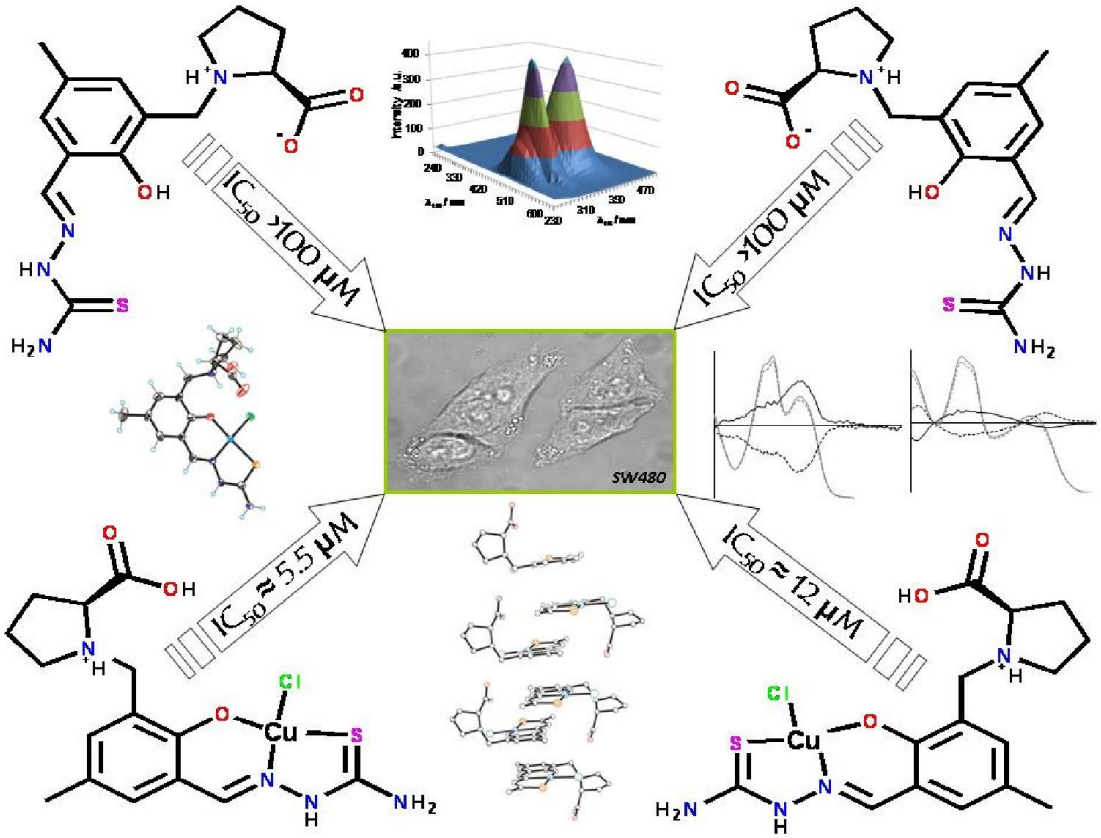

The copper(II) complexes [Cu(*L*-Pro-STSC)Cl]Cl and [Cu(*L*-Pro-STSC)Cl]Cl are 13 and 5 times more potent antiproliferative agents in CH1 cells than the free thiosemicarbazone-proline conjugates *L*-Pro-STSC and *D*-Pro-STSC based on comparison of IC_{50} values. The difference in cytotoxicity in SW480 cells is even higher.